A&A 670, A127 (2023)
https://doi.org/10.1051/0004-6361/202244783

Astronomy & Astrophysics

The 100-month *Swift* catalogue of supergiant fast X–ray transients

II. SFXT diagnostics from outburst properties

P. Romano[1], P. A. Evans[2], E. Bozzo[3,4], V. Mangano[1], S. Vercellone[1], C. Guidorzi[5,6,7], L. Ducci[8,3], J. A. Kennea[9], S. D. Barthelmy[10], D. M. Palmer[11], H. A. Krimm[12], and S. B. Cenko[10]

[1] INAF – Osservatorio Astronomico di Brera, Via E. Bianchi 46, 23807 Merate, Italy
e-mail: patrizia.romano@inaf.it
[2] University of Leicester, X-ray and Observational Astronomy Group, School of Physics & Astronomy, University Road, Leicester, LE1 7RH, UK
[3] Department of Astronomy, Université de Genève, 16 chemin d'Écogia, 1290 Versoix, Switzerland
[4] INAF – Osservatorio Astronomico di Roma, Via Frascati, 33, 00078 Monte Porzio Catone, Rome, Italy
[5] Department of Physics and Earth Science, University of Ferrara, Via Saragat 1, 44122 Ferrara, Italy
[6] INFN – Sezione di Ferrara, Via Saragat 1, 44122 Ferrara, Italy
[7] INAF – Osservatorio di Astrofisica e Scienza dello Spazio di Bologna, Via Piero Gobetti 93/3, 40129 Bologna, Italy
[8] Institut für Astronomie und Astrophysik, Kepler Center for Astro and Particle Physics, Universität, Tübingen, Sand 1, 72076 Tübingen, Germany
[9] Department of Astronomy and Astrophysics, Pennsylvania State University, University Park, PA 16802, USA
[10] Astrophysics Science Division, NASA Goddard Space Flight Center, Greenbelt, MD 20771, USA
[11] Los Alamos National Laboratory, B244, Los Alamos NM 87545, USA
[12] National Science Foundation, Alexandria, VA 22314, USA

Received 20 August 2022 / Accepted 6 December 2022

ABSTRACT

Supergiant fast X-ray transients (SFXTs) are high mass X-ray binaries (HMXBs) displaying X-ray outbursts that can reach peak luminosities up to 10^{38} erg s^{-1} and spend most of their lives in more quiescent states with luminosities as low as 10^{32}–10^{33} erg s^{-1}. During the quiescent states, less luminous flares are also frequently observed with luminosities of 10^{34}–10^{35} erg s^{-1}. The main goal of the comprehensive and uniform analysis of the SFXT *Swift* triggers presented in this paper is to provide tools to predict whether a transient that has no known X-ray counterpart may be an SFXT candidate. These tools can be exploited for the development of future missions exploring the variable X-ray sky through large field-of-view instruments. We examined all available data on outbursts of SFXTs that triggered the *Swift*/Burst Alert Telescope (BAT) collected between 2005 August 30 and 2014 December 31, in particular those for which broad-band data, including the *Swift*/X-ray Telescope (XRT) data, are also available. This work complements and extends our previous catalogue of SFXT flares detected by BAT from 2005 February 12 to 2013 May 31, since we now include the additional BAT triggers recorded until the end of 2014 (i.e. beyond the formal first 100 months of the *Swift* mission). Due to a change in the mission's observational strategy, virtually no SFXT triggers obtained a broad-band response after 2014. We processed all BAT and XRT data uniformly by using the *Swift* Burst Analyser to produce spectral evolution dependent flux light curves for each outburst in the sample. The BAT data allowed us to infer useful diagnostics to set SFXT triggers apart from the general γ-ray burst population, showing that SFXTs uniquely give rise to image triggers and are simultaneously very long, faint, and 'soft' hard-X-ray transients. We find that the BAT data alone can discriminate very well the SFXTs from other classes of fast transients, such as anomalous X-ray pulsars and soft gamma repeaters. On the contrary, the XRT data collected around the time of the BAT triggers are shown to be decisive for distinguishing SFXTs from, for instance, accreting millisecond X-ray pulsars and jetted tidal disruption events. The XRT observations of 35 (out of 52 in total) SFXT BAT triggers show that in the soft X-ray energy band, SFXTs display a decay in flux from the peak of the outburst of at least three orders of magnitude within a day and rarely undergo large re-brightening episodes, favouring in most cases a rapid decay down to the quiescent level within three to five days (at most).

Key words. X-rays: binaries – catalogs

1. Introduction

Supergiant fast X-ray transients (SFXTs) are high mass X-ray binaries (HMXBs) associated with OB supergiants set apart from the classical supergiant HMXBs–which show luminosity variations by a factor of 10–50 on time scales of a few hundred to thousands of seconds–for a distinctive dynamic range up to 10^5 times larger (SFXTs; e.g. for recent reviews, see Walter et al. 2015; Martínez-Núñez et al. 2017). With a quiescent level of $\sim 10^{32}$ erg s^{-1} (e.g. in't Zand 2005; Bozzo et al. 2010) and peak luminosities up to 10^{38} erg s^{-1} (Romano et al. 2015a), the SFXT dynamic range can reach up to six orders of magnitude, despite SFXTs being overall significantly sub-luminous with respect to classical supergiant HMXBs (Lutovinov et al. 2013; Bozzo et al. 2015). SFXTs indeed go through rare outbursts that can last up to a few days (as is the case of IGR J11215−5952,

Table 1. Sample of SFXTs and candidates.

Name	Spectral type	Distance (kpc)	P_{spin} (s)	P_{orb} (d)	P_{sup} (d)	Eclipse	e	Ref. Disc	Sp.T.	D	References P_{spin}	P_{orb}; e	P_{sup}	Eclipse
(1)	(2)	(3)	(4)	(5)	(6)	(7)	(8)	(9)	(10)	(11)	(12)	(13)	(14)	(15)
IGR J08408−4503	O8.5Ib-II(f)p	$2.20^{+0.08}_{-0.09}$	–	9.5436 ± 0.0002	285±10	N	0.63 ± 0.03	1	2	3	–	4; 4	4	–
IGR J11215−5952	B0.5Ia	$7.06^{+0.55}_{-0.56}$	186.78 ± 0.3	164.6	–	N	>0.8	5	6	3	7	8; 9	–	–
IGR J16328−4726	O8Iafpe	7.2±0.3	–	10.076 ± 0.003	–	N	–	10	11	12	–	13	–	–
IGR J16418−4532	BN0.5Ia	13	1209.12 ± 0.42	3.73886 ± 0.00003	14.730 ± 0.006	Y	–	14	15	15	16	17	18	19
IGR J16465−4507 [a]	B0.5Ib/O9.5Ia	$9.4/9.5^{+14.1}_{-5.7}$	228 ± 6	30.243 ± 0.035	–	N	<0.6,<0.8	23	21,15	15,22	23	24; 25	–	–
IGR J16479−4514	O8.5I	4.45	–	3.3193 ± 0.0005	11.880 ± 0.002	Y	–	26	15	27	–	28	18	29
XTE J1739−302	O8Iab(f)	2.01±0.16	–	51.47 ± 0.02 [b]	–	N	<0.8	30,31	32	3	–	33; 33	–	–
IGR J17544−2619	O9Ib	3.0±0.2	71.49 ± 0.02 [c]	4.926 ± 0.001	–	N	>0	34	35	36	37	38; 38	–	–
SAX J1818.6−1703	O9I-B1I	2.1 ± 0.1	–	30 ± 0.1	–	N	0.3–0.4	39	40	41	–	42,43; 43	–	–
AX J1841.0−0536	B1Ib	$3.2^{+2.0}_{-1.5}$,6.9 ± 1.7	4.7394 ± 0.0008? [d]	6.4565±0.0055 [e]	–	N	–	44,45	22	22,46	45	47	–	–
AX J1845.0−0433	O9.5I	6.4 ± 0.76	–	5.7195 ± 0.0007	–	N	<0.37	48	49	50	–	51; 51	–	–
IGR J18483−0311 1	B0.5Ia/B0-B1Iab	2.83 ± 0.05	21.0526 ± 0.0005 [f]	18.545 ± 0.003	–	N	0.4	52	15,41	41	53	54,17; 55	–	–
2XMM J185114.3 [g]	–	12	–	–	–	–	–	56,57	–	58	–	–	–	–

Notes. Binary properties and optical counterparts. [a]Classical HMXB, not considered further. [b]See Romano et al. (2009b, P_{orb} = 12.8658 ± 0.0073 d). [c]See Romano et al. (2015a, P_{spin} = 11.6 ± 0.13 s). [d]See Bozzo et al. (2011). [e]Tentative. [f]See Ducci et al. (2013). [g]Candidate SFXT.

References. (1) Götz et al. (2006); (2) Sota et al. (2014); (3) Bailer-Jones et al. (2021); (4) Gamen et al. (2015); (5) Lubinski et al. (2005); (6) Vijapurkar & Drilling (1993); (7) Swank et al. (2007); (8) Romano et al. (2009c); (9) Lorenzo et al. (2014); (10) Bird et al. (2007); (11) Coleiro et al. (2013); (12) Persi et al. (2015); (13) Corbet et al. (2010); (14) Tomsick et al. (2004); (15) Rahoui et al. (2008); (16) Drave et al. (2013); (17) Levine et al. (2011); (18) Corbet & Krimm (2013); (19) Corbet et al. (2006); (20) Lutovinov et al. (2004); (21) Negueruela et al. (2007); (22) Nespoli et al. (2008); (23) Lutovinov et al. (2005); (24) La Parola et al. (2010); (25) Clark et al. (2010); (26) Molkov et al. (2003); (27) Arnason et al. (2021); (28) Romano et al. (2009b); (29) Bozzo et al. (2008a); (30) Smith et al. (1997); (31) Smith et al. (1998); (32) Negueruela et al. (2006); (33) Drave et al. (2010); (34) Sunyaev et al. (2003); (35) Pellizza et al. (2006); (36) Gimenez-Garcia et al. (2016); (37) Drave et al. (2012); (38) Clark et al. (2009); (39) in't Zand et al. (1998); (40) Negueruela & Schurch (2007); (41) Torrejón et al. (2010); (42) Bird et al. (2009); (43) Zurita Heras & Chaty (2009); (44) Bamba & Koyama (1999); (45) Bamba et al. (2001); (46) Sguera et al. (2009); (47) González-Galán (2015); (48) Yamauchi et al. (1995); (49) Coe et al. (1996); (50) Coleiro & Chaty (2013); (51) Goossens et al. (2013); (52) Chernyakova et al. (2003); (53) Sguera et al. (2007); (54) Levine & Corbet (2006); (55) Romano et al. (2010a); (56) Watson et al. (2009); (57) Lin et al. (2012); (58) Romano et al. (2016).

Romano et al. 2007) characterised by bright flares that typically last a few hours (Sguera et al. 2005; Romano et al. 2007, 2014a; Paizis & Sidoli 2014; Sidoli & Paizis 2018; Sidoli et al. 2019), timescales that are significantly shorter than those observed in Be/X-ray binaries (see, e.g., Reig 2011, for a review). As with classical systems hosting accreting neutron stars (NS), the hard X-ray spectra during outbursts are power laws combined with high energy cut-offs, reminiscent of those of HMXBs, so it is generally assumed that all SFXTs might host an NS. Indeed, in about half of the SFXT sample (see Table 1) a pulsation is observed that is interpreted as an NS spin period, and cyclotron resonant scattering features (CRSF) have been proposed but never confirmed (see Sguera et al. 2010 and Ducci et al. 2013 for IGR J18483−0311, Bhalerao et al. 2015 and Bozzo et al. 2016 for IGR J17544−2619, and Sidoli et al. 2017, 2020 for IGR J11215−5952).

The detailed physics behind the SFXT outbursts is still unknown, but it is probably related to either the properties of the wind from the supergiant companion (in't Zand 2005; Walter & Zurita Heras 2007; Negueruela et al. 2008; Sidoli et al. 2007; Ducci et al. 2009, 2010; Bozzo et al. 2021) or the compact object itself, an NS, with the presence of mechanisms inhibiting accretion (Grebenev & Sunyaev 2007; Bozzo et al. 2008b). The most recent development (Shakura et al. 2012, 2014) includes a subsonic settling accretion regime combined with magnetic reconnections between the NS and the supergiant field transported by its wind (see also Hubrig et al. 2018).

The brightest flares from the SFXTs have been triggering the Burst Alert Telescope (BAT; Barthelmy et al. 2005) on board the *Neil Gehrels Swift* Observatory (Gehrels et al. 2004) since just after its launch. *Swift*'s unique properties of automatic fast-slewing and broad-band energy coverage have made it the sole observatory that can not only detect these events from the very beginning, but it also enables the tracking of their evolution for days with a sensitive focusing X-ray instrument, the X-ray Telescope (XRT; Burrows et al. 2005).

In general, when a triggering event is recognised as originating from a previously known source (i.e. when it is in the on-board BAT catalogue), *Swift* does not slew to the target. For new or 'special interest' sources, however, *Swift* performs a slew so that the narrow-field-instrument (NFI) can also image the target and provide broad-band data. This has been the case for SFXTs since 2008 September 25 when, in order to ensure simultaneous NFI data, the *Swift* team enabled automatic rapid slews to a pre-defined set of these objects following detection of flares by BAT, as is routinely done for γ-ray bursts (GRBs). Furthermore, the triggering threshold for SFXTs was also lowered after each outburst so as to allow further GRB-like response. This strategy has quickly tripled the available sets of data on SFXT outbursts and allowed arc-second localisation with the XRT of several confirmed SFXTs and a number of candidate sources in this class whose coordinates were previously only known at the arc-minute level (e.g. Kennea et al. 2005; Kennea & Campana 2006; Romano et al. 2016). This consequently helped the firm association of these objects with an optical/infrared counterpart. Further details and a review of the *Swift* SFXT Project can be found in Romano (2015). Several bright flares were also independently caught by the BAT Transient Monitor[1] (Krimm et al. 2013a) and observed with the XRT during the monitoring campaigns that were performed on four SFXTs between 2007 and 2009 (Romano et al. 2011a, and references therein).

[1] http://swift.gsfc.nasa.gov/docs/swift/results/transients/

On 2012 May 14, the BAT triggering threshold was lowered from 6.4 to 5.8 σ in order to better hunt for short (see, e.g. Kouveliotou et al. 1993) GRBs. As a beneficial side effect, this also resulted in more detections of soft γ-ray repeaters (SGRs) and SFXTs. For the latter sources, this change allowed BAT to be triggered by the faint flares of IGR J16418−4532 on 2012 June 3, 2013 April 2, and 2015 April 27; by fainter flares from IGR J17544−2619 on 2012 July 24 and 2013 June 28; and by XTE J1739−302 on 2012 September 9 and 2012 November 11 (see Table 2). Starting from the end of 2014, the threshold for a slew for SFXTs was not lowered after each outburst; consequently, only increasingly brighter events were granted a GRB-like response, enabling broad-band data collection. The triggering statistics changed dramatically, and this resulted in virtually no additional SFXT triggers with broad-band data after 2014.

In a companion paper (Romano et al. 2014a, Paper I), we presented the catalogue of 1117 flares defined as detections in excess of 5σ registered by both the BAT on board *Swift* and the BAT Transient Monitor on the ground (Krimm et al. 2013a), regardless of whether broad-band data were collected or not with the *Swift* NFI. These events were recorded from 11 SFXTs between 2005 February 12 and 2013 May 31. We showed that these flares/outbursts lasted just a few hundred seconds, achieving average fluxes as large as 100 mCrab, (15–50 keV) and average luminosities in the range 10^{34}–10^{35} erg s^{-1}. Based on our results, and in combination with the first nine years of INTEGRAL/ISGRI data (Paizis & Sidoli 2014), Ducci et al. (2014) derived the expected number of SFXTs emitting bright flares in the Milky Way, $N \approx 37^{+53}_{-22}$, revealing that SFXTs may constitute a large portion of supergiant X-ray binaries (XRBs) in the Galaxy. Given that the SFXT class currently includes only about a dozen confirmed individuals, it is appropriate to devise methods to find the SFXTs still undetected.

In this paper (Paper II), we focus on the bright SFXT flares that triggered the BAT and for which complementary broad-band XRT data were also simultaneously collected. The aim of our analysis is to exploit a uniform dataset of combined BAT+XRT data for its predictive potential. In Sect. 2, we describe our samples and the uniform processing of the BAT and XRT data with the Burst Analyser (Evans et al. 2010) to produce spectral evolution dependent flux light curves. In Sect. 3, we derive some characteristic properties of SFXTs as a sample both in the hard and in the soft X-ray band, and we discuss our findings, considering future perspectives, thus tackling the issue of predicting whether a Galactic transient that has no known X-ray counterpart may be an SFXT candidate for *Swift* and for other future missions exploring the X-ray variable sky with large field-of-view instruments. We examine several diagnostics that help identify SFXT candidates among the population of newly discovered fast X-ray transients. Finally, in Sect. 4, we summarise our findings and draw our conclusions.

2. Data sample, reduction, and analysis

2.1. The SFXT sample

Our sample of SFXTs was selected from the literature based on reports of bright flares (peak $L \gtrsim 10^{36}$ erg s^{-1}) recorded by ASCA, RXTE, INTEGRAL, and *Swift* (their properties were detailed in Paper I, Sect. 2). Given the different timescales and dynamic ranges on which the SFXT activity is observed, it is appropriate to recapitulate our distinction between a flare, which is a state of enhanced emission generally lasting for a few hours (average luminosities in the range 10^{34}–10^{35} erg s^{-1}; Paper I), and an outburst, which is composed of several very bright flares (reaching luminosities up to $\sim 10^{38}$ erg s^{-1}) that can last, depending on the source, up to a day or longer. It is also worth briefly re-stating that our operative definitions of 'confirmed' and 'candidate' SFXTs are based on the availability (or lack thereof) of an optical classification of the companion. Hence, a confirmed SFXT is a transient that has shown repeated, large dynamical range flaring/outbursting activity and is firmly associated with an OB supergiant, while a candidate SFXT is a transient that has shown similar X-ray behaviour but has no confirmed association with an OB supergiant companion.

Table 1 lists the information for all SFXTs considered in Paper I, updated according to the most recent literature, regarding spectral type and distance; the spin, orbital, and super-orbital periods; the presence of eclipses in the X-ray light curve; orbital eccentricities; and the references to discovery and counterpart properties. Different from Table 3 of Paper I, IGR J16465−4507 (which never triggered the BAT) was found to be a classical HMXB and not an SFXT (Romano et al. 2014b), while the source 2XMM J185114.3−000004 has been included in our sample as a promising SFXT candidate (Romano et al. 2016). We note that IGR J11215−5952 also never triggered the BAT, so it is not considered in this work.

Also different from Paper I, the sample of outbursts actually exceeds the first 100 months of the *Swift* mission and includes all recorded outbursts until the end of 2014 (thus including three triggers that occurred after 2013 May 31 and five that occurred during 2014). In Table 2, we summarise the *Swift* observations of the 11 sources that triggered the BAT or for which outbursts where observed in the X-ray with XRT during our monitoring campaigns. The table reports the progressive number of triggers, the BAT trigger number, the BAT trigger significance of detection, trigger UT dates, the kind of data available for each outburst, the references to the discovery, and the in-depth outburst analysis when already published. We also note the instances (four) where subsequent bright flares within the same outburst triggered the BAT.

From launch to the end of December 2014, *Swift*/BAT detected 52 outbursts (for a total of 56 on-board triggers). Of these, 35 have broad-band coverage, a great majority of which (27) have this coverage thanks to the SFXTs being added to the BAT special interest source list[2].

2.2. The GRB sample

Because GRBs are the main triggering sources for the BAT, they make a natural control sample for the SFXT one. For this work, we considered all GRBs that triggered the BAT until the end of 2014 (839 triggers). The data from *Swift*-detected GRBs are regularly processed with the *Swift* Burst Analyser (Evans et al. 2010), which ensures uniformity in treatment with SFXTs.

[2] For completeness, we note that two SFXT outbursts were also detected from IGR J16418−4532 after the end of 2014: one on 2015 April 27 (trigger 639 199, Barthelmy et al. 2015; Romano et al. 2015b), which based on the ground-based analysis revealed a significance much smaller than the one derived on board so that XRT only observed the normal out-of-outburst activity for this source, and one on 2021 September 18 (trigger 1 073 821, Sbarufatti et al. 2021). The latter event will be considered separately in a forthcoming publication.

Table 2. *Swift* SFXT outburst data.

Name		Trigger				Data		References	
	N[a]	#[b]	S/N[c]	UT Date	UT Time	BAT ObsID	XRT ObsID	Discovery	Refereed
(1)	(2)	(3)	(4)	(5)	(6)	(7)	(8)	(9)	(10)
IGR J08408−4503	1	232 309	8.08	2006-10-04	14:45:43	00232309000	00232309000,001	1	2,3
	2	316 063	7.38	2008-07-05	21:14:13	00316063000	00316063000,00030707003–012	4	3
	3	325 461	10.00	2008-09-21	07:55:09	00325461000	00325461000,00030707013–018	5,6	7
	4	361 128[d]	6.62	2009-08-28	22:51:47	00361128000	00030707019	8	9
	5	361 129[d]	10.26	2009-08-28	23:09:23	00361129000	–	8	9
	6	417 420	8.68	2010-03-28	15:53:38	00417420000	00417420000	10	9
	7	501 368	7.28	2011-08-25	00:53:05	00501368000	00501368000,00037881002–011	11	9
	8	559 642	7.16	2013-07-02	08:10:45	00559642000	00559642000,00037881097–102	12	–
IGRJ 16328−4726	1	354 542	7.69	2009-06-10	07:54:27	00354542000	00354542000–004	13	14,15
	2	510 701	7.87	2011-12-29	06:39:20	00510701000	–	–	16
IGR J16418−4532	1	307 208	7.23	2008-03-21	23:01:33	00307208000	–	–	16
	2	523 489	6.22	2012-06-03	18:08:48	00523489000	00523489000–001	17	18
	3	552 677	6.39	2013-04-02	11:56:30	00552677000	00552677000	19	16
	4	571 067	7.26	2013-09-17	14:41:17	00571067000	00571067000,00032037008–014	20	–
IGR J16479−4514	1	152 652	7.71	2005-08-30	04:08:48	00152652000	00152652000,00030296001–004	21	22,23,24
	2	210 886	5.78	2006-05-20	17:32:39	00210886000	–	25	23
	3	215 914	5.34	2006-06-24	20:19:59	00215914000	–	23	23
	4	286 412	9.98	2007-07-29	12:07:34	00286412000	–	23	23
	5	306 829[e]	12.02	2008-03-19	22:44:45	00306829000	00306829000,00030296029–033	26,27	28
	6	306 830[e]	21.64	2008-03-19	22:59:57	00306830000	–	27	28
	7	312 068	7.21	2008-05-21	06:03:41	00312068000	–	–	29
	8	341 452	10.68	2009-01-29	06:33:08	00341452000	00341452000,00030296077–095	30,31	32,29
	9	599 041	17.22	2014-05-15	09:52:45	00599041000	–	33	–
XTE J1739−302	1	282 535	6.53	2007-06-18	03:10:46	00282535000	–	–	23
	2	308 797	7.83	2008-04-08	21:28:13	00308797000	00308797000	34	35
	3	319 963[f]	9.15	2008-08-13	23:49:17	00319963000	00319963000,00030987070–081	36	7
	4	319 964[f]	11.14	2008-08-14	00:12:53	00319964000	–	36	7
	5	346 069	6.81	2009-03-10	18:39:55	00346069000	00030987106–109	37	38
	6	446 475	7.44	2011-02-22	07:21:37	00446475000	00446475000	39	40
	7	533 120	5.81	2012-09-09	23:34:14	00533120000	00533120000,00030987192–195	41	16
	8	538 084	6.10	2012-11-11	09:35:02	00538084000	–	42	16
IGR J17544−2619		BTM	–	2007-11-08	01:31:04	–	–	43	16
	1	308 224	9.10	2008-03-31	20:50:45	00308224000	00308224000,00035056021	44	35
		XRT	–	2008-09-04	00:19:00	–	00035056061	45	7
		BTM	–	2009-03-15	23:52:40	–	–	46	38
	2	354 221	8.15	2009-06-06	07:48:59	00354221000	00354221000–1,00035056109–111	47	38
	3	414 875	7.45	2010-03-04	23:13:54	00414875000	00414875000–1,0035056149	48	49
	4	449 907	12.78	2011-03-24	01:56:57	00449907000	00449907000,00035056150–152	50	40
		BTM	–	2012-04-12	00:37:20	–	00035056153–155	51	16
	5	528 432	6.14	2012-07-24	04:52:47	00528432000	00528432000	52	16
	6	559 221	6.02	2013-06-28	07:26:21	00559221000	00559221000	53	54
	7	570 402	13.78	2013-09-11	15:59:49	00570402000	00570402000	55	54
	8	599 954[g]	9.23	2014-05-25	22:25:48	00599954000	00599954000,00035056156–160	56,57	–
	9	599 955[g]	11.30	2014-05-25	22:33:08	00599955000	00599955000	–	–
	10	614 903	19.82	2014-10-10	15:04:19	00614903000	00614903000,00035056161–166	58,59	54
		BTM	–	2015-02-21	11:21:20	–	00035056167–168	60	–

Notes. [a]Progressive number of BAT trigger. [b]BAT Trigger number. [c]On-board significance of detections of BAT trigger in units of σ. [d–g]The source triggered the BAT twice within a few minutes.

References. (1) Ziaeepour et al. (2006); (2) Götz et al. (2007); (3) Romano et al. (2009a); (4) Palmer et al. (2008); (5) Mangano et al. (2008b); (6) Mangano et al. (2008a); (7) Sidoli et al. (2009a); (8) Barthelmy et al. (2009); (9) Mangano et al. (2012); (10) Romano et al. (2010c); (11) Mangano et al. (2011b); (12) Romano et al. (2013f); (13) Grupe et al. (2009); (14) Fiocchi et al. (2010); (15) Romano et al. (2013a); (16) Romano et al. (2014a); (17) Romano et al. (2012d); (18) Romano et al. (2013b); (19) Romano et al. (2013d); (20) Krimm et al. (2013b); (21) Kennea et al. (2005); (22) Kennea (2006); (23) Sidoli et al. (2008a); (24) Sguera et al. (2008); (25) Markwardt & Krimm (2006); (26) Barthelmy et al. (2008b); (27) Romano et al. (2008b); (28) Romano et al. (2008a); (29) Romano et al. (2009b); (30) Romano et al. (2009d); (31) La Parola et al. (2009); (32) Bozzo et al. (2009); (33) Romano (2014); (34) Romano et al. (2008c); (35) Sidoli et al. (2009c); (36) Romano et al. (2008d); (37) Romano et al. (2009e); (38) Romano et al. (2011a); (39) Romano et al. (2011c); (40) Farinelli et al. (2012a); (41) Romano et al. (2012h); (42) D'Elia et al. (2012); (43) Krimm et al. (2007); (44) Sidoli et al. (2008b); (45) Romano et al. (2008e); (46) Krimm et al. (2009); (47) Romano et al. (2009g); (48) Romano et al. (2010b); (49) Romano et al. (2011b); (50) Romano et al. (2011d); (51) Romano et al. (2012b); (52) Romano et al. (2012f); (53) Romano et al. (2013e); (54) Romano et al. (2015a); (55) Romano et al. (2013g); (56) Barthelmy et al. (2014a); (57) Romano et al. (2014c); (58) Barthelmy et al. (2014b); (59) Romano et al. (2014d); (60) Krimm & Romano (2015); (61) Barthelmy et al. (2008a); (62) Romano et al. (2009f); (63) Sidoli et al. (2009b); (64) Romano et al. (2009i); (65) Romano et al. (2012a); (66) Romano et al. (2009j); (67) Kennea et al. (2014); (68) de Pasquale et al. (2010); (69) Romano et al. (2010d); (70) Mangano et al. (2011a); (71) Romano et al. (2012e); (72) Romano et al. (2012g); (73) Romano et al. (2009h); (74) Romano et al. (2012c); (75) Krimm et al. (2011); (76) Barthelmy et al. (2012); (77) Romano et al. (2016).

Table 2. continued.

Name		Trigger			Data			References	
	N[(a)]	#[(b)]	*S/N*[(c)]	UT Date	UT Time	BAT ObsID	XRT ObsID	Discovery	Refereed
(1)	(2)	(3)	(4)	(5)	(6)	(7)	(8)	(9)	(10)
SAX J1818.6−1703	1	294 385	7.94	2007-10-16	04:14:30	00294385000	–	–	16
	2	306 379	8.02	2008-03-15	15:49:01	00306379000	–	61	16
	3	351 323	7.12	2009-05-06	14:02:11	00351323000	00351323000,00031409001–010	62	63
	4	361 958	6.63	2009-09-05	11:15:15	00361958000	00361958000	64	65
	5	374 869	7.34	2009-11-04	07:24:11	00374869000	–	66	16
	6	591 551	6.16	2014-03-13	08:28:20	00591551000	00591551000	67	–
AX J1841.0−0536	1	423 958	6.87	2010-06-05	17:23:30	00423958000	00423958000–1,00030988093–101	68,69	49
	2	455 967	6.91	2011-06-24	14:27:05	00455967000	00030988107–114	70	16
	3	524 364	8.47	2012-06-14	19:11:52	00524364000	00524364000,00030988115–120	71	18
	4	528 411	9.81	2012-07-24	00:40:15	00528411000	00528411000	72	16
AX J1845.0−0433	1	162 526	5.43	2005-11-04	22:26:48	00162526000	–	–	16
	2	355 911	6.99	2009-06-28	08:06:03	00355911000	00355911000	73	16
	3	521 567	7.26	2012-05-05	01:44:40	00521567000	00521567000–001,00032456001–023	74	15
IGR J18483−0311	1	321 750	11.48	2008-08-24	10:48:29	00321750000	–	–	16
		BTM	–	2011-11-23		–	–	75	16
2XMM J185114.3	1	524 542	7.11	2012-06-17	15:46:56	00524542000	00524542000–005,007–017	76	77

2.3. Other transients

It is also worthwhile to consider other transients, both Galactic and extragalactic, that share the ability to trigger the BAT as well as some timing, energetics, and/or spectral properties.

For instance, the jetted tidal disruption event (TDE) *Swift* J164449.3+573451 (Burrows et al. 2011) that repeatedly triggered the BAT starting from 2011 March 28 (Cummings et al. 2011; Suzuki et al. 2011; Sakamoto et al. 2011) showed characteristics reminiscent of SFXTs during its first day of discovery (Kennea et al. 2011b). Similarly, the millisecond pulsar (MSP) IGR J18245−2452 (Papitto et al. 2013) showed an initial soft X-ray light curve similar to a that of an SFXT (Romano et al. 2013c). In Table A.1, we report the BAT triggers from these two sources: the progressive number of triggers, the BAT trigger number, the BAT trigger significance of detection, the trigger UT dates, the references to the discovery and the in-depth outburst analysis, and the source type.

We also considered representative objects in the anomalous X-ray pulsars (AXPs) and soft gamma repeaters (SGRs) class listed in the McGill Online Magnetar Catalog[3] (Olausen & Kaspi 2014) that triggered the BAT. Table A.2 reports, as a few examples, the trigger data of the Galactic magnetar SGR 1935+2154, which was first discovered by *Swift* (Cummmings et al. 2014), as well as two prototypical supergiant HMXBs, Vela X-1 and 4U 1909+07 (see, e.g. Kretschmar et al. 2019, for a recent review) that are known for showing conspicuous flares (see Walter et al. 2015, and references therein).

Finally, we note that the outbursts of SFXTs can be easily distinguished from those of most Be HMXBs and black hole candidates because the latter two are usually caught while the source flux is still rising and the whole outburst lasts considerably longer, from days to months (see, e.g. Kennea 2015, and Kennea et al. 2011a, 2021, and references therein). In contrast, SFXT light curves return to pre-outburst levels within a few hours or a day. Therefore, we do not discuss Be HMXBs and black hole candidate flares any further.

[3] http://www.physics.mcgill.ca/~pulsar/magnetar/main.html

2.4. The Swift Burst Analyser

All SFXT data collected after a standard (i.e. GRB-like) BAT trigger were processed with a minimally[4] modified version of the *Swift* Burst Analyser[5] (Evans et al. 2010), whose methods we only summarise here while highlighting the special arrangements made for the case of SFXTs, whose properties differ from those of GRBs for which it was intended. The *Swift* Burst Analyser uses scripts based on FTOOLS[6] and the calibration database CALDB[7] to manipulate the event data of GRB BAT triggers collected by BAT and XRT. By using the hardness ratio information in each instrument, it tracks the spectral evolution and converts the count-rate light curves from both BAT and XRT into accurate, evolution-corrected flux light curves. Figure 1 shows an example of the products of the Burst Analyser, which are the BAT+XRT flux density light curves at 10 keV (Fig. 1f).

The BAT data are processed with the tool BATGRBPRODUCTS, which yields information that we can later use as diagnostics. In keeping with the GRB terminology to define the typical timescales and energetics of the emission, this information includes the trigger time T_0 (measured in mission elapsed time, MET, i.e. seconds since 2001-01-01), which is the origin of the time ($t = T + T_0$, where t is in MET and T is in seconds since the trigger), and T_{90}, the time during which 90% of the fluence is emitted (from 5 to 95%). The tool also calculates the fluences (in units of on-axis counts per fully illuminated detectors) in the standard BAT energy bands, 15–25, 25–50, and 50–100 keV, which can be used to calculate hardness ratios and colours (see Evans et al. 2010, for further details). Examples of this procedure for SFXTs are the BAT 25–50 keV/15–25 keV hardness ratios (Fig. 1b) and the 15–50 keV spectral evolution dependent fluxed light curves (Fig. 1d).

To convert the count-rate light curves into spectral evolution dependent flux light curves, a time-evolving counts-to-flux

[4] The SFXT version of the code uses XRT hardness ratios different from the GRB version, due to the harder spectra of these latter objects.
[5] http://www.swift.ac.uk/burst_analyser
[6] https://heasarc.gsfc.nasa.gov/ftools/ftools_menu.html
[7] https://heasarc.gsfc.nasa.gov/docs/heasarc/caldb/caldb_intro.html

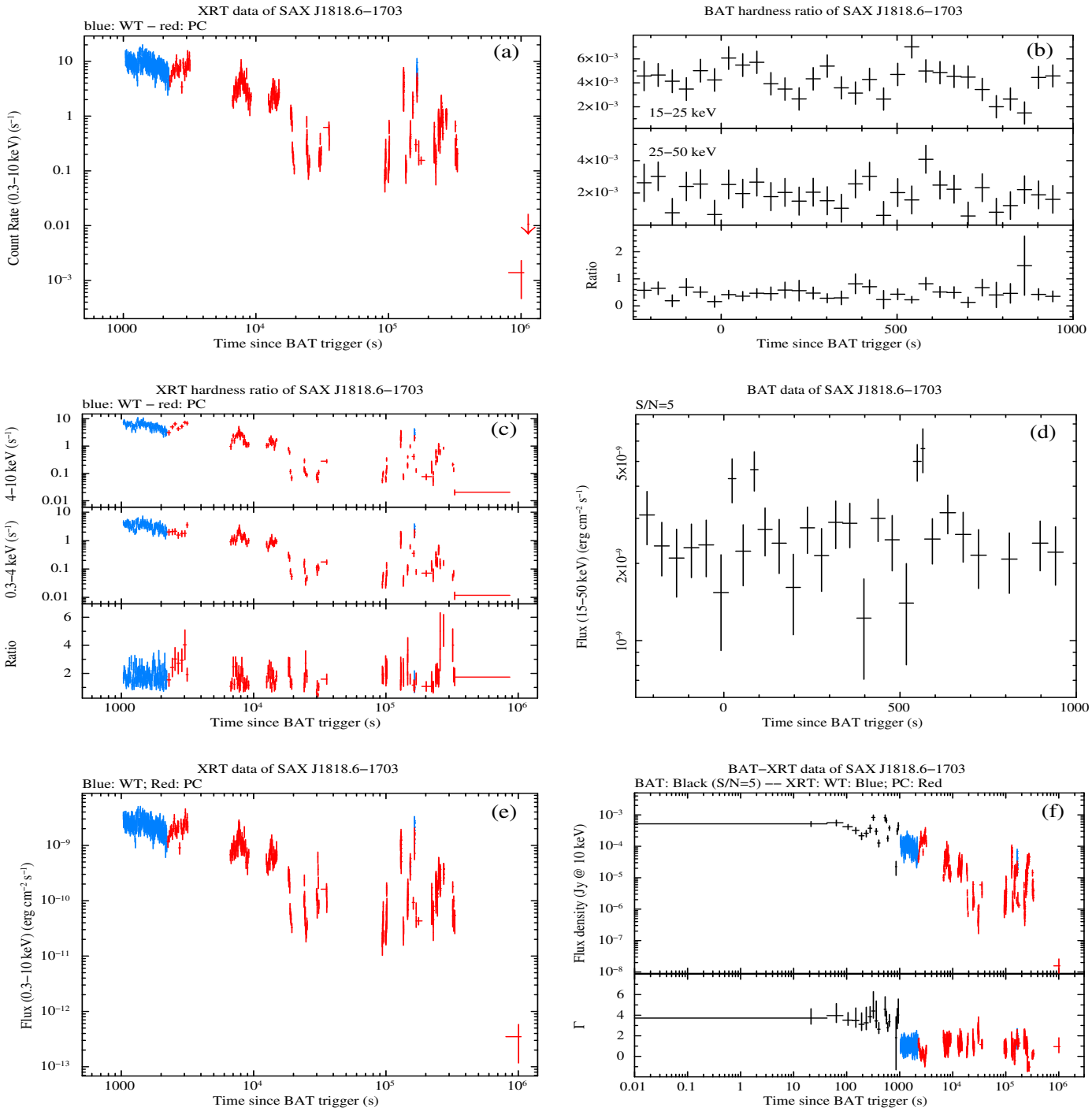

Fig. 1. Example of Burst Analyser products for the third recorded outburst from SAX J1818.6−1703 (see Table 2). (a) XRT 0.3–10 keV count-rate light curve; (b) BAT 15–25 keV, 25–50 keV, and (25–50 keV/15–25 keV) hardness ratio; (c) XRT 4–10 keV, 0.3–4 keV and (4–10 keV/0.3–4 keV) hardness ratio; (d) BAT 15–50 keV spectral evolution dependent flux light curve; (e) XRT 0.3–10 keV spectral evolution dependent, unabsorbed flux light curve; (f) evolution dependent flux density light curves at 10 keV.

conversion factor is required for BAT and XRT, separately, and with a single HR per instrument, only one free parameter can be derived. As the sources are generally too faint in the BAT band to provide time-resolved spectroscopy, a spectral shape is assumed and the hardness ratios are used to track the evolution. Therefore, a single spectrum is created for all available BAT data, and this is fitted with both a power-law and cut-off power-law spectral model. If the latter gives a χ^2 value of at least nine lower than the former (i.e. a 3σ improvement), then the cut-off power-law model is used to determine the counts-to-flux conversion factor. The cut-off energy is assumed not to vary.

The XRT data are similarly processed with the tool XRTPIPELINE and, as described in full in Evans et al. (2007, 2009), light curves are created in the standard XRT energy bands (0.3–1.5, 1.5–10, 0.3–10 keV for GRBs; 0.3–4, 4–10, 0.3–10 keV for SFXTs). The hardness ratio 1.5–10 keV/0.3–1.5 keV

(4–10 keV/0.3–4 keV for SFXTs) is also created (e.g. Figs. 1a and 1c).

For XRT the Burst Analyser adopts an absorbed power law with an absorption model consisting of two components, PHABS in XSPEC (Arnaud 1996): one fixed at the Galactic column density (Kalberla et al. 2005) and one representing the local absorption. The absorption is therefore determined by extracting a spectrum from all available XRT data corresponding to the trigger and fitting an absorbed power-law model to this spectrum. As with the cut-off energy, this absorption is thereafter assumed to be unchanging as the flare progresses.

For each of the BAT and XRT spectra, the determined spectral model is loaded into XSPEC, and the photon index of the (cut-off) power law, Γ, is varied in the range -2.5 to five. A look-up table is thus created (for each Γ value) of the hardness ratio, the unabsorbed 0.3–10 keV flux, the unabsorbed 15–50 keV flux, the model normalisation, and the count rate predicted by the model. From those data, the hardness ratios versus count-rate-to-flux conversion factors are calculated. Figure 1f, bottom panel, reports the photon indices.

The normalisations of the power-law and cut-off power-law models in XSPEC are defined as the photon flux density at 1 keV in units of photons $\mathrm{cm^{-2}\,s^{-1}\,keV^{-1}}$. In terms of energy flux density normalisation, 1 keV ($\mathrm{cm^{-2}\,s^{-1}\,keV^{-1}}$) is thus equivalent to 662.5 μJy. This can then be extrapolated to give the flux density at 10 keV (Fig. 1f, top panel). By interpolating within the look-up tables, the hardness ratios can be converted into time evolution histories of count-rate-to-flux conversion factors. Further details can be found in Evans et al. (2010, 2007, 2009). We note that we chose 10 keV for the flux density since it is an intermediate energy between the XRT and BAT bands; hence, the extrapolation was minimal.

We note that approximations were made (i.e. a constant absorption for the XRT spectra and a constant energy of the cut-off for the BAT spectra), but the impact on our results is negligible. In Table 2, we report the references for the in-depth analysis of each dataset, specifically tailored to the SFXT case, where the broad-band spectroscopy is performed with several spectral models (also with a cut-off energy as a free parameter) and absorption variations sought for. We stress that variable absorbing column densities during a flare were rarely observed in the XRT data (e.g. Romano et al. 2007, 2009a; Sidoli et al. 2009a). In general (e.g. Romano et al. 2011a, 2014b), they are not very strongly supported by the data, save for rare cases, since the XRT effective area is too small to measure fast variations on shorter timescales that can be probed by higher effective area instruments, such as the EPIC cameras on board *XMM–Newton*, with which truly remarkable variations have been measured (e.g. Bozzo et al. 2017).

Discussing the ensemble of the detailed analyses reported in Table 2 is beyond the scope of this paper, so we refer the reader to the appropriate references where it was performed, justified by the fact that the spectroscopic properties are not an efficient method for discriminating SFXTs within the HMXB population (e.g. Romano 2015), which is different from what happens for the dynamic range, as we show in Sect. 3.4. Indeed, the practice is to fit the SFXT spectra (broad band or single band) with models that apply to NS binaries. Even the models that were specifically developed for SFXTs, such as the physical model `compmag` in XSPEC (Farinelli et al. 2012b), which includes thermal and bulk Comptonization for cylindrical accretion onto a magnetised NS, can be successfully applied to not only the SFXT prototypes XTE J1739−302 and IGR J17544−2619 (Farinelli et al. 2012a) and IGR J18483−0311 (Ducci et al. 2013) but also to several magnetised accreting pulsars (e.g. Farinelli et al. 2016).

Table 3. Improved X-ray positions.

Name [(a)]	RA (J2000)	Dec (J2000)	Error
IGR J08408−4503	08 40 47.77	−45 03 30.5	1.″4
IGR J16328−4726	16 32 37.87	−47 23 42.4	1.″4
IGR J16418−4532	16 41 50.90	−45 32 26.7	1.″4
IGR J16465−4507	16 46 35.28	−45 07 05.2	1.″9
AX J1845.0−0433	18 45 01.62	−04 33 56.6	1.″4

Notes. [(a)]The positions for the full SFXT sample can be found in Table 1 of Paper I.

2.5. Improved X-ray positions from XRT data

For all sources observed by *Swift*, independent of whether they triggered the BAT or not, we derived astrometrically corrected X-ray positions by using the XRT-UVOT alignment and matching to the USNO-B1 catalogue (Monet et al. 2003), as described in Goad et al. (2007) and Evans et al. (2009)[8]. Table 3 reports the cases where this new processing produced improved X-ray positions (significantly smaller 90%-confidence error circles[9]), compared to previous publications in the literature. These are currently the best X-ray positions for this subset of SFXTs, although they are compatible with previous results within the uncertainties.

3. Results and discussion

Currently, most new Galactic transients are either discovered in deep hard X-ray surveys (i.e. INTEGRAL/IBIS and *Swift*/BAT) or as previously unknown or unidentified sources that trigger hard X-ray monitors and GRB-chasing missions (such as *Swift* and MAXI). Since our ultimate goal is to provide a set of diagnostics to discriminate SFXT candidates from newly discovered hard X-ray transients, we first characterised the SFXT 'transient' behaviour in terms of length of emission, fluences, and spectral properties and then compared them with the corresponding behaviours of GRBs and other relevant Galactic and extragalactic transients. We exploited the observed diagnostics in the chronological order they became available to us, starting from the information distributed through the Gamma-ray Coordinates Network[10] (GCN) Notices[11] and then proceeded with information that could only be derived through the analysis of the transient downlinked data.

3.1. SFXTs are image triggers

As we discussed in Paper I, the BAT on-board trigger algorithm (Fenimore et al. 2003) works on several different timescales and has three types of triggers. Two triggers are based on increases of count rates (short rate triggers on timescales of 4–64 ms; long rate triggers, 64 ms–24 s), and one trigger is based on images (image triggers, 64 s to many minutes). In the case of image

[8] http://www.swift.ac.uk/user_objects/
[9] See https://www.swift.ac.uk/user_objects/docs.php#posform
[10] https://gcn.gsfc.nasa.gov/
[11] https://www.swift.ac.uk/gcn/index.php

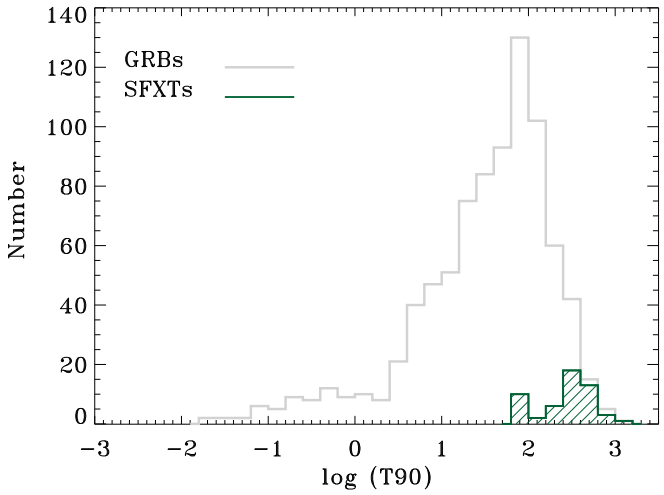

Fig. 2. Distribution of T_{90}. T_{90} (s) are calculated by the Burst Analyser for SFXT triggers (N = 53), represented by hashed dark green histogram, and for GRB triggers (N = 839) represented by a light grey line.

triggers, significant sources are sought in each image, and if the source is known and its image flux exceeds a threshold set in the on-board source catalogue, then *Swift* will slew to it. For known SFXTs, the on-board threshold was set very low until the end of 2014 so that *Swift* would respond with a slew whenever the SFXTs became significantly brighter. The type of trigger (rate vs. image) and its duration are included in the information distributed with the GCN Notices, within seconds to minutes from the trigger.

All SFXT triggers recorded on board are image triggers. The image length in which SFXTs are generally triggering varies from 64 to 1600 s, the latter being the longest continuous pointing *Swift* can perform, hence the longest timescale available for image creation[12]. In contrast, based on our analysis of 839 triggers, GRBs are detected as image triggers only about 13% of the time. Both *Swift* J164449.3+573451 and IGR J18245−2452 produced image triggers, lasting from 64 s to 1208 s for the former and from 64 s to 320 s for the latter, and events such as these are not easily set apart from the SFXT population based on the triggering method only. On the contrary, AXPs/SGRs and magnetar flares are all rate triggers with durations from 0.008 to 0.128 s; hence, they can be set apart from the SFXT phenomenology by merely hundreds of seconds after the trigger.

We also note that the SFXTs IGR J08408−4503, IGR J16479−4514, XTE J1739−302, and IGR J17544−2619 have sometimes triggered the BAT twice within about an hour (more often within a few minutes; see Table 2), indicating that the source flux is steadily rising. While double triggers can occur in jetted TDEs (e.g. *Swift* J164449.3+573451) and most commonly in Galactic transients (see Table A.1), they are very uncommon in GRBs. However, they may occur in the so-called ultra-long GRBs, which are indeed rare in the observed GRB population (Levan et al. 2014).

3.2. SFXTs are very long transients

The second diagnostic we considered, calculated from the transient downlinked and ground-processed data (hence hours since the trigger) by the Burst Analyser, is T_{90}. In Fig. 2 we compare the GRB sample (N_1 = 839), with its two peaks caused by the short and long GRB populations (see, e.g. Kouveliotou et al. 1993), and the SFXT sample. The overall range, based on all usable data points ($N_{\rm TOT}$ = 53), is between 64 s and 1344 s, and he mean is 338±32 s. Some of these points (N = 30) are, however, derived from the Tracking and Data Relay Satellite System (TDRSS) on-board values, as the algorithm calculating T_{90} converged on the image duration (BATTBLOCKS failed). The strictly 'ground-calculated' sample (N_2 = 23) yielded a range of 92–795 s and a mean of 429±40 s.

We note that most of the ground-calculated T_{90} for SFXTs are also to be considered realistically lower limits since they are based on BAT event mode data only, which are telemetered to the ground, typically from T_0-239 s to T_0+963 s. Indeed, BAT often registers an emission not only well before the trigger but also for several hundred seconds after the event list ends, as shown in the survey mode data collected by the BAT. SFXTs therefore could fall on the high-end tail of the T_{90} distribution and should therefore be compared with long GRBs.

We performed a Kolmogorov-Smirnov test (Darling 1957; Press et al. 1992) on the GRB (N_1 = 839) and the complete SFXT (N_2 = 53) samples of T_{90} and obtained a K-S statistic D_{N_1,N_2} = 0.651 and a K-S probability of 2×10^{-19}, showing that the two underlying one-dimensional probability distributions differ significantly. Even when excluding all GRBs with T_{90} < 10 s (effectively excluding short GRBs), $D_{656,53}$ = 0.622 and the K-S probability is 1×10^{-17}, thus confirming that the T_{90} of SFXTs and long GRBs are not drawn from the same parent distribution. When considering the strictly ground-calculated sub-sample, we found $D_{839,23}$ = 0.810 and a probability of 6×10^{-14}, while $D_{656,23}$ = 0.780 and a probability 7×10^{-13}, so our conclusions were not modified by the use of the complete SFXT sample.

As a comparison, the jetted TDE Swift J164449.3+573451 and the MSP IGR J18245−2452 have T_{90} in the 64–1208 s and 55–120 s range, respectively. Therefore, such events are not distinguishable from the SFXT population based on their T_{90} only.

At odds with SFXT flares, AXPs/SGRs and magnetar flares have T_{90} in the 0.008–950 s range, but most of them are below one second. Therefore, even when a triggering algorithm did not include image triggers, AXPs/SGRs and magnetar flares would not be confused with SFXTs because of their short duration.

3.3. SFXTs are faint and 'soft' hard-X-ray transients

The energetics of transients are customarily described by the fluence in several bands, which the Burst Analyser calculates in units of on-axis counts per fully illuminated detector. We considered the 15–25 keV (soft), 25–50 keV (medium), and 50–100 keV (hard) energy bands, measured fluences for both SFXTs and GRBs and calculated the corresponding colours: $S_{21} = S(25-50)/S(15-25)$ and $S_{31} = S(50-100)/S(15-25)$.

The average SFXT fluences in the soft band are consistent with those of GRBs, with the $S(15-25)_{\rm SFXT} = 1.76 \pm 0.42$ cts det^{-1} and $S(15-25)_{\rm GRB} = 1.68 \pm 0.18$ cts det^{-1}, but they are significantly fainter than GRBs above 25 keV, which are in the medium and hard bands. Indeed, they emit most of their hard X-ray energy in the 15–25 keV range then, in increasingly lower proportion, in the medium and hard bands in a manner similar to the GRB subset of X-ray flashes (Heise et al. 2001; Sakamoto et al. 2005, 2008; D'Alessio et al. 2006). Consequently, the SFXT hardness ratios are systematically larger for

[12] Fig. 2 of Paper I shows the durations of the BAT triggers and a comparison with the BAT flares registered both on board and on the ground.

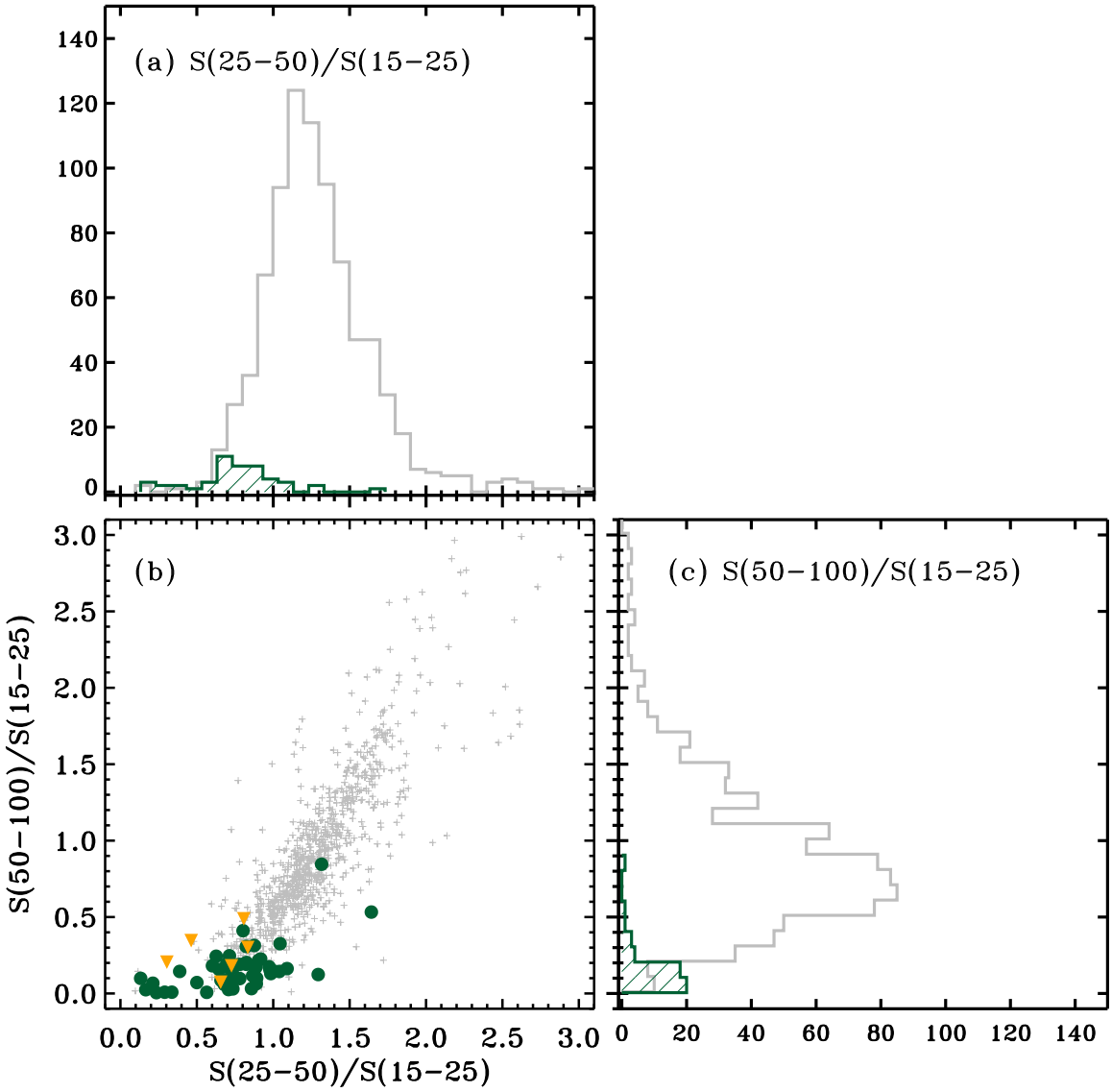

Fig. 3. Energetics. Comparison of energetics of SFXT (N = 48, dark green) and GRB (N = 833, grey): (a) distributions of the S_{21} = $S(25-50)/S(15-25)$ colours; (b) colour-colour diagram drawn from the 15–25 keV, 25–50 keV, and 50–100 keV energy bands, with the orange triangles (N = 6) representing 3 σ upper limits for $S(50-100)$; (c) distributions of the S_{31} = $S(50-100)/S(15-25)$ colours.

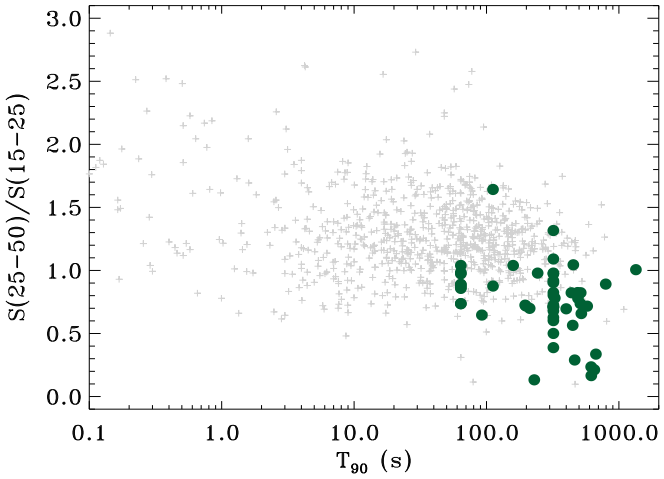

Fig. 4. Colours vs. T_{90}. Dark green filled circles are the SFXTs; light grey crosses are the GRBs.

GRBs than for SFXTs, $S_{21,\mathrm{GRB}} = 1.31 \pm 0.02$ and $S_{31,\mathrm{GRB}} = 0.97 \pm 0.02$, $S_{21,\mathrm{SFXT}} = 0.76 \pm 0.04$ and $S_{31,\mathrm{SFXT}} = 0.15 \pm 0.02$, although both are affected by large errors.

Figure 3b shows the colour-colour diagram comparing the SFXT sample to the GRB sample. Figures 3a and 3c show the distributions of the S_{21} and S_{31} colours, respectively. A K-S test for S_{21} yielded a statistic $D_{833,48} = 0.693$ and a probability of 4×10^{-20} and for S_{31} a statistic $D_{833,48} = 0.867$ and a probability of 3×10^{-31}, showing that the two underlying one-dimensional probability distributions differ significantly. For comparison, Fig. A.1 shows the corresponding values for the TDE Swift J164449.3+573451 and the MSP IGRJ 18245−2452, the magnetar SGR 1935+2154, the two SgHMXBs Vela X−1, and 4U 1909+07.

In order to further distinguish SFXTs from GRBs, in Figs. 4 and 5 we plot the fluence ratio S_{21} and S_{31} as a function of T_{90}, respectively. In particular, Fig. 5 shows the faintness of SFXTs relative to GRBs in the hard band, which is a useful property in terms of discriminating these two classes.

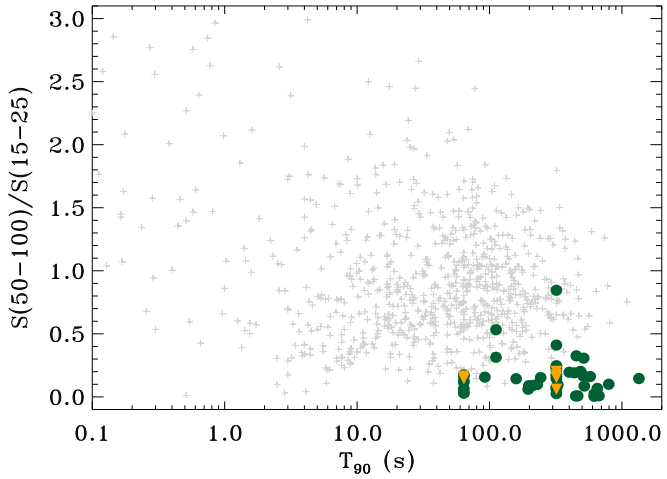

Fig. 5. Colours vs. T_{90}. Dark green filled circles are the SFXTs, orange triangles ($N = 6$) represent SFXT $3\,\sigma$ upper limits for $S(50-100)$, and light grey crosses are the GRBs.

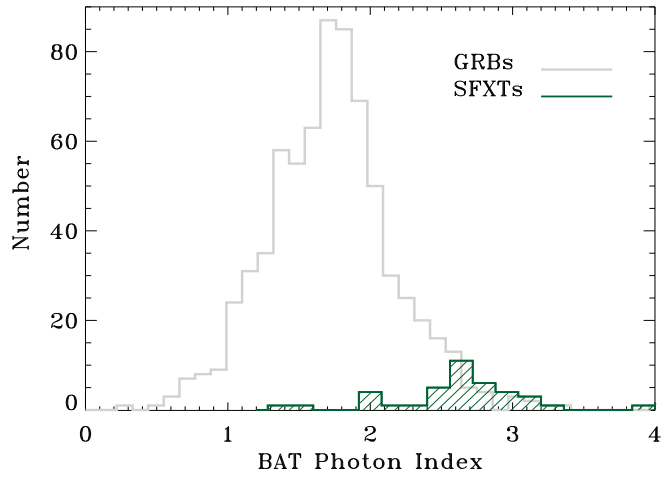

Fig. 6. Distribution of photon indices for SFXT triggers (hashed green histogram) and GRBs (light grey histogram) when BAT spectra are fit with a simple power-law model.

The Burst Analyser performed fits of the BAT event data during the whole available time interval. For SFXTs the spectra are best fit with simple power laws in 42 out of 53 cases, with photon indices ranging between 1.4 and 4.7 and with a mean of $\Gamma_{\rm SFXT} = 2.77 \pm 0.11$. Such soft indices in the BAT band are customary (e.g. Romano et al. 2008a), confirming the findings of most works based on INTEGRAL data (see Sidoli & Paizis 2018, and references therein). The distribution of photon indices is shown in Fig. 6 as a hashed dark green histogram. The light grey histogram is the distribution of photon indices of GRBs that are best fit with a simple power law ($N_1 = 709$). The mean is $\Gamma_{\rm GRB} = 1.72 \pm 0.02$. A K-S test for Γ yielded a statistic $D_{709,42} = 0.746$ and a probability of 2×10^{-20}, showing that the SFXTs and GRBs photon indices are not drawn from the same parent distribution. This implies that the BAT spectra of SFXTs are significantly softer than those of GRBs. In particular, we note that SFXT photon indices resemble those typical of X-ray flashes (e.g. Sakamoto et al. 2008). SFXTs are therefore described by relatively faint and soft long transients.

3.4. Soft X-ray prompt and longer-term variability

As described in Sect. 2.1, 35 outbursts (out of 52 events) offer a broad-band coverage. In this section, we consider the XRT data for their potential to help predict the outlook of prospective soft X-ray observations following a hard X-ray trigger. Figure 7 shows the 0.3–10 keV count-rate light curves for each BAT trigger (see Table 2) arranged by object[13]. Clearly, the light curves are very complex and there is no obvious common behaviour, as their evolution varies among different sources and often even among different outbursts of the same source. However, there is an overall trend for a fast decay, by up to three orders of magnitude in a few hours. Re-brightening, in the form of subsequent multiple flares can also occur, as previously reported (e.g. Romano et al. 2007, 2009a; Sidoli et al. 2008a). We also note that after about one day after the trigger, there is a flattening of the general trend towards the mean value for these sources (see Romano et al. 2011a, 2014b).

Figure 8 shows the count-rate light curves on the same time scale, seconds since the BAT trigger. To characterise the overall behaviour, we calculated the median of all light curve points in a given time interval with the time intervals equal in logarithmic space. We note that this trend, due to the presence of many orbital and data gaps in the light curves and multiple flares, needs to be taken with caution, as it depends on the time intervals selected.

Figure 9 shows the spectral evolution dependent unabsorbed flux light curves obtained with the methods described in Sect. 2.4 all together. Similar to what was observed in Fig. 8, we note that the only shared trait is the lack of a common behaviour, with the exception of a general fast decay in flux by orders of magnitude in a few hours. Although, as stated previously, the mean trend needs to be taken with caution, we can still exploit its predictive power in terms of the expected flux at a given time after the BAT trigger, as is done for GRBs (e.g. Evans et al. 2009, Fig. 11, and Margutti et al. 2013, Table 3).

Finally, Fig. 10 shows the unabsorbed luminosity light curves, which are based on the spectral evolution dependent flux light curves previously described and the distances reported in Table 1. We only propagated the errors on fluxes and not those on distances, as the latter were often just an estimate or were missing altogether.

By using the count rate and spectral evolution dependent flux light curves, we could calculate the maximum and minimum in flux and the respective dynamical ranges in the 0.3–10 keV energy band for each of the considered SFXTs. These data are reported in Table 4, where we also indicate the time from the BAT trigger at which the source minimum flux was recorded.

In the soft X-ray domain (0.3–10 keV), the combination of a fast variability, a several orders of magnitude flux decay in just a few hours, and the lack of any major re-brightening within the following few days (see Table 4, Figs. 8, and 10) remain key identification criteria for objects in the SFXT class. Excluding GRBs that can otherwise already be discriminated by exploiting virtually only BAT data (see previous sections), the other classes of transient and variable sources considered for comparison with the SFXTs in this paper show largely different behaviours in the XRT energy domain. AXPs/SGRs display much steadier light curves over time (see, e.g. Esposito et al. 2021, and references therein), and the AMXP IGR J18245−2452 was characterised

[13] We note that the XRT data of the 2008-03-19 outburst of IGR J16479−4514 start earlier than the BAT trigger since, at the time, we were monitoring the source regularly (Romano et al. 2008a).

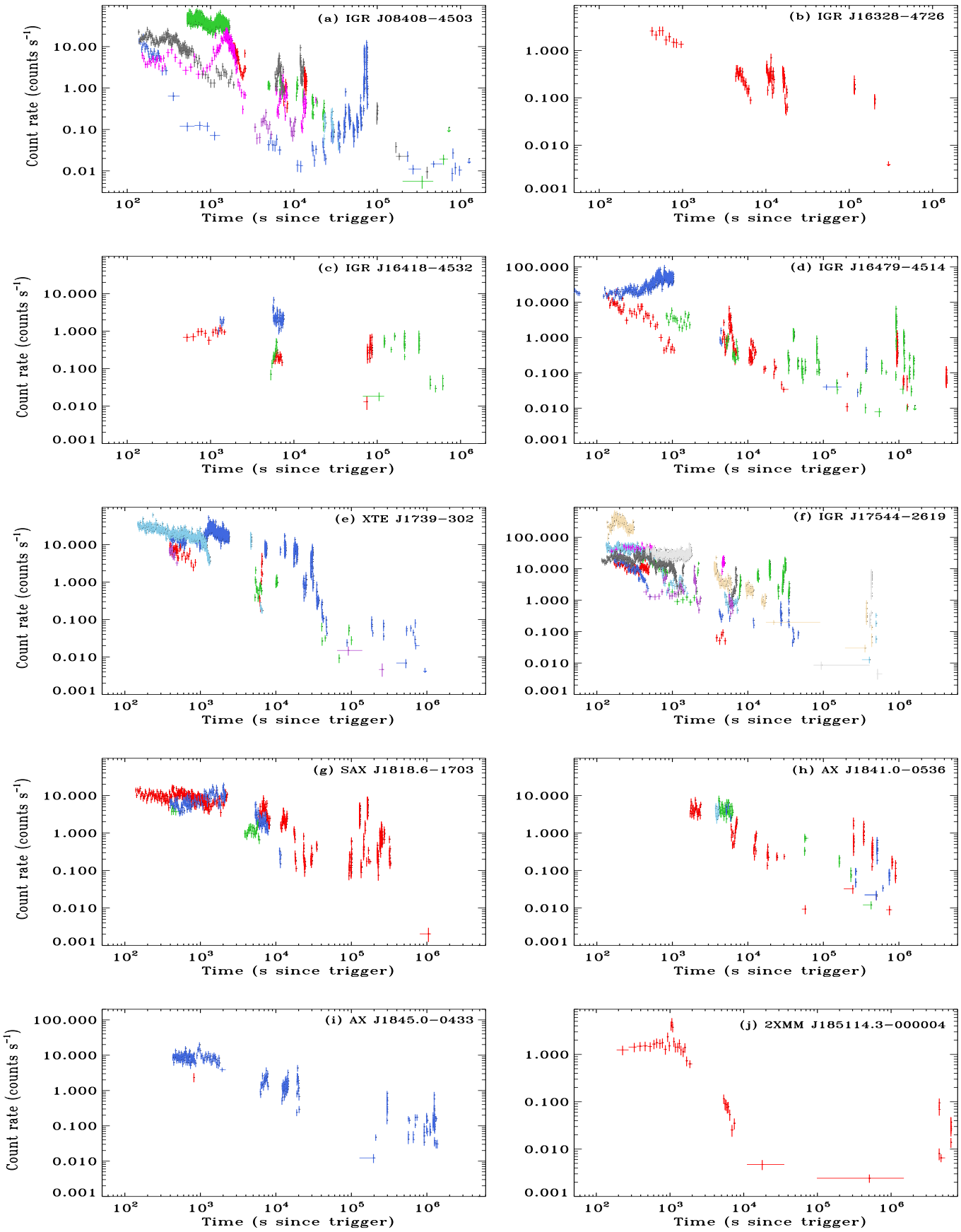

Fig. 7. XRT light curves (counts s^{-1}) in the 0.3–10 keV energy band grouped by source [(a) IGR J08408−4503, (b) IGR J16328−4726, (c) IGR J16418−4532, (d) IGR J16479−4514, (e) XTE J1739−302, (f) IGR J17544−2619, (g) SAX J1818.6−1703, (h) AX J1841.0−0536, (i) AX J1845.0−0433, (j) 2XMM J185114.3−000004] as a function of time (s) since the BAT trigger, where different colours correspond to different events. The complete list of triggers for each source can be found in Table 2.

Table 4. *Swift*/XRT maximum and minimum count rates (counts s^{-1}) and dynamical ranges and maximum and minimum fluxes (erg cm^{-2} s^{-1}) and dynamical ranges.

Name	CR_{max}	CR_{min} 10^{-3}	CR DR	$Flux_{max}$ $\times10^{-10}$	$Flux_{min}$ $\times10^{-13}$	Flux DR	$Time_{min}$ (d)
(1)	(2)	(3)	(4)	(5)	(6)	(7)	(8)
IGR J08408−4503	73.5 ± 11.1	5.6 ± 1.9	13012.4 ± 4861.2	$109.3^{+16.6}_{-16.9}$	7.1 ± 2.4	15348.0 ± 5739.9	4.0
IGR J16328−4726	2.6 ± 0.6	<4.6	573.7	7.7 ± 1.7	203.1 ± 42.3	38.2 ± 11.7	0.2
IGR J16418−4532	$47.9^{+8.2}_{-8.0}$	13.1 ± 5.2	3658.3 ± 1580.1	$80.0^{+13.6}_{-13.4}$	$120.5^{+26.5}_{-26.5}$	664.1 ± 184.9	5.8
IGR J16479−4514	$96.8^{+17.3}_{-14.7}$	7.9 ± 2.3	12257.8 ± 4162.1	$278.1^{+49.7}_{-44.7}$	16.9 ± 4.9	16490.9 ± 5599.8	6.4
XTE J1739−302	61.7 ± 9.2	$4.6^{+2.1}_{-1.7}$	13289.4 ± 6332.9	166.9 ± 24.9	$7.3^{+3.3}_{-2.6}$	22732.2 ± 10832.8	3.0
IGR J17544−2619	$604.8^{+130.0}_{-126.2}$	$4.5^{+1.9}_{-1.5}$	133484.1 ± 63140.9	$772.6^{+166.1}_{-161.2}$	$5.7^{+2.4}_{-1.9}$	136374.7 ± 64508.2	6.0
SAX J1818.6−1703	19.3 ± 2.9	$2.0^{+0.9}_{-0.8}$	9450.3 ± 4500.9	43.3 ± 6.5	$5.1^{+2.3}_{-2.0}$	8573.3 ± 4087.2	12.1
AX J1841.0−0536	8.4 ± 1.5	9.0 ± 2.6	938.5 ± 317.4	14.3 ± 3.1	17.0 ± 4.1	840.8 ± 271.7	5.0
AX J1845.0−0433	19.8 ± 3.4	12.3 ± 3.5	1609.2 ± 532.3	32.1 ± 5.5	20.0 ± 5.7	1604.0 ± 530.6	2.3
2XMM J185114.3	4.8 ± 1.1	2.4 ± 0.5	1969.6 ± 591.9	20.6 ± 4.6	28.0 ± 6.7	736.7 ± 241.6	0.2

Notes. All are measured in the 0.3–10 keV energy band from the light curves described in Sect. 3.4. We also indicated the time after the BAT trigger at which the minimum source flux was recorded.

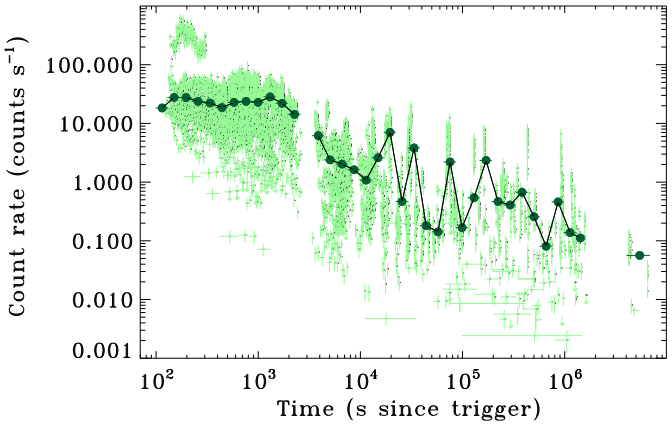

Fig. 8. XRT count-rate light curves (counts s^{-1}) in 0.3–10 keV energy band as a function of time (s since the BAT trigger). The dark green points mark the medians.

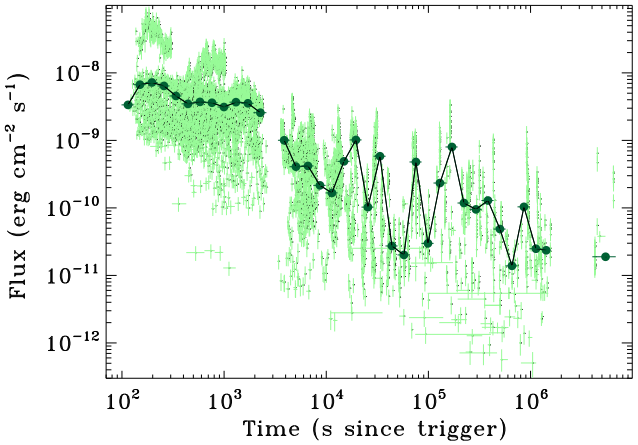

Fig. 9. XRT unabsorbed flux light curves (erg cm^{-2} s^{-1}) in the 0.3–10 keV energy band as a function of time (s since the BAT trigger). The dark green points mark the medians.

during its outburst by a much slower decrease of the average X-ray flux (a few days rather than hours; Ferrigno et al. 2014). The peculiar case of the TDE *Swift* J164449.3+573451 showed the necessity of monitoring the transients for at least a few days with XRT to set the event apart from an SFXT candidate. The XRT data collected up to within a day of the BAT trigger still showed the TDE to closely resemble an SFXT (Kennea et al. 2011b), but on a longer term (a few days), the XRT data displayed the presence of multiple major re-flares and re-brightening that do not occur in SFXTs (see, e.g. Burrows et al. 2011). The simultaneous availability of prompt XRT detection and monitoring of a few days with the *Swift* NFI following the BAT trigger can therefore provide the most solid ground to identify promising SFXT candidates.

4. Conclusions

In this paper, which complements our previous catalogue of SFXT outbursts detected by BAT in the first 100 months of the *Swift* mission (Romano et al. 2014a, Paper I), we considered all BAT and XRT data collected as an outburst or as an outburst

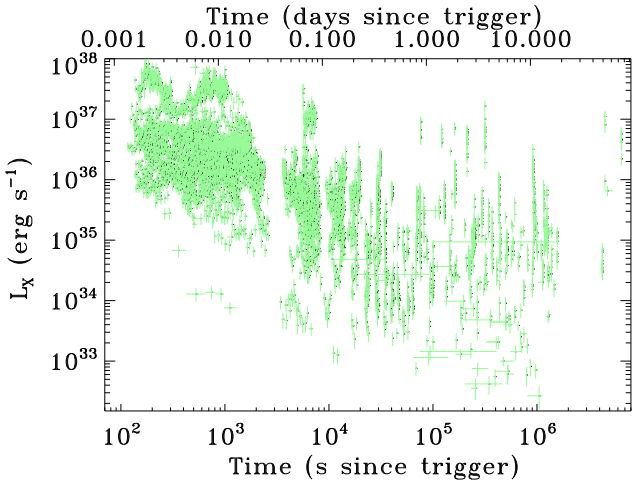

Fig. 10. XRT unabsorbed luminosity light curves (erg s^{-1}) in the 0.3–10 keV energy band as a function of time (s since the BAT trigger).

follow-up. Our dataset consists of 52 outbursts (for a total of 56 on-board triggers), of which 35 have broad-band coverage, the great majority of which (27) is due to SFXTs being labelled as special sources for the BAT. We processed the datasets uniformly with the *Swift* Burst Analyser and exploited them to derive a set of diagnostics that would help distinguish SFXT triggers in future missions scanning the variable X-ray sky with large field-of-view instruments. In particular, we concentrated in setting SFXTs apart from the overwhelmingly abundant population of GRBs, especially in the time periods just after the trigger. Our systematic investigation of all SFXT outbursts that triggered the *Swift*/BAT led us to the following findings:

- All SFXT triggers recorded on board BAT are image triggers.
- SFXTs are very long transients. The durations range between 64 s and 1344 s, with a mean of 338 ± 32 s. The T_{90} of SFXTs and long GRBs are not drawn from the same parent distribution.
- The SFXTs are faint hard-X-ray transients. Most of the SFXT fluence is found in the 15–25 keV band; however, SFXTs are fainter than GRBs in both the 15–25 keV and 25–50 keV bands.
- The SFXTs are 'soft' hard-X-ray transients. The BAT spectral indices are systematically softer than those of GRBs. The mean values are $\Gamma_{\rm SFXT} = 2.77 \pm 0.11$ and $\Gamma_{\rm GRB} = 1.72 \pm 0.02$. The photon indices of SFXTs and GRBs are not drawn from the same parent distribution.
- The SFXT properties in the BAT energy band (both fluences and spectral indices) more closely resemble those of X-ray flashes, which are generally much shorter transients than SFXTs.
- The SFXT X-ray light curves show a common trend for a fast decay, by up to three orders of magnitude, in a few hours after the trigger and a flattening after about one day after the trigger. Multiple flaring activity was also observed, leading to a re-brightening up to a few days after the trigger. The dynamical ranges in the soft X-rays reach six orders of magnitude (IGR J17544−2619, see Romano et al. 2015a). By exploiting the XRT data accumulated up to 2014 as part of the *Swift* triggering observational strategy for SFXTs, we found that the combination of the SFXT variability in the soft X-ray domain with their fast decay in flux during the first few hours after the trigger and continuous decay in the following few days is a distinguishable fingerprint for these objects. Thus, the XRT data can be efficiently used to set SFXTs apart not only from GRBs (already possible by using virtually only BAT data) but also from other transients, such as AXPs/SGRs, AMXPs, and jetted TDEs.

In summary, we find that SFXTs can already be set apart from the overall GRB population relatively well by exploiting BAT trigger data because SFXTs give rise to image triggers that are very long, faint, and 'soft' in the hard-X-ray domain. The prompt distinction of candidate SFXTs from other classes of transients, such as AMXPs and jetted TDEs, most likely requires the availability of XRT data from seconds after the trigger and up to at least a few days. This allows the investigation of the most typical SFXT fingerprint, consisting of a fast variability in the soft X-ray domain and both a decay in flux by several orders of magnitude within hours after the onset of the outburst and a steady decay in the following days.

As mentioned earlier in this paper, the threshold for a *Swift* slew for SFXTs was no longer lowered after each outburst after 2014. Consequently, only increasingly brighter outbursts were given a GRB-like response in more recent years, which enabled the unique prompt broad-band data coverage provided by the exploitation of both the BAT and XRT. Unless the strategy changes again, the present dataset is unlikely to be significantly extended further.

Acknowledgements. We thank M. Capalbi, D. Malesani, and C. Ferrigno for helpful discussions. We acknowledge unwavering support from Amos. We also thank the anonymous referee for comments that helped to improve the paper. We acknowledge financial contribution from contracts ASI-INAF I/004/11/0, ASI-INAF I/037/12/0, and ASI-INAF n. 2017-14-H.0, H.A.K. acknowledges support while serving at the National Science Foundation. The data underlying this article are publicly available from the *Swift* archive. This work made use of data supplied by the UK Swift Science Data Centre at the University of Leicester. The *Swift*/BAT transient monitor results are provided by the *Swift*/BAT team. Happy 18th, *Swift*.

References

Arnason, R. M., Papei, H., Barmby, P., Bahramian, A., & Gorski, M. D. 2021, MNRAS, 502, 5455
Arnaud, K. A. 1996, ASP Conf. Ser., 101, 17
Bailer-Jones, C. A. L., Rybizki, J., Fouesneau, M., Demleitner, M., & Andrae, R. 2021, AJ, 161, 147
Bamba, A., & Koyama, K. 1999, IAU Circ., 7324, 4
Bamba, A., Yokogawa, J., Ueno, M., Koyama, K., & Yamauchi, S. 2001, PASJ, 53, 1179
Barthelmy, S. D., Barbier, L. M., Cummings, J. R., et al. 2005, Space Sci. Rev., 120, 143
Barthelmy, S. D., Krimm, H. A., Markwardt, C. B., Palmer D. M., & Ukwatta, T. N. 2008a, GCN Circ., 7419, 1
Barthelmy, S. D., Baumgartner, W. H., Burrows, D. N., et al. 2008b, GCN Circ., 7466, 1
Barthelmy, S. D., Romano, P., Burrows, D. N., et al. 2009, ATel, 2178, 1
Barthelmy, S. D., Baumgartner, W. H., Burrows, D. N., et al. 2012, GCN Circ., 13367, 1
Barthelmy, S. D., Burrows, D. N., D'Elia, V., et al. 2013, GCN Circ., 14355, 1
Barthelmy, S. D., Cenko, S. B., D'Elia, V., et al. 2014a, GCN Circ., 16330, 1
Barthelmy, S. D., Bernardini, M. G., Burrows, D. N., et al. 2014b, GCN Circ., 16904, 1
Barthelmy, S. D., Beardmore, A. P., Cummings, J. R., et al. 2015, GCN Circ., 17764, 1
Bhalerao, V., Romano, P., Tomsick, J., et al. 2015, MNRAS, 447, 2274
Bird, A. J., Malizia, A., Bazzano, A., et al. 2007, ApJS, 170, 175
Bird, A. J., Bazzano, A., Hill, A. B., et al. 2009, MNRAS, 393, L11
Bozzo, E., Stella, L., Israel, G., Falanga, M., & Campana S. 2008a, MNRAS, 391, L108
Bozzo, E., Falanga, M., & Stella, L. 2008b, ApJ, 683, 1031
Bozzo, E., Giunta, A., Stella, L., et al. 2009, A&A, 502, 21
Bozzo, E., Stella, L., Ferrigno, C., et al. 2010, A&A, 519, A6
Bozzo, E., Giunta, A., Cusumano, G., et al. 2011, A&A, 531, A130
Bozzo, E., Romano, P., Ducci, L., Bernardini, F., & Falanga, M. 2015, Adv. Space Res., 55, 1255
Bozzo, E., Bhalerao, V., Pradhan, P., et al. 2016, A&A, 596, A16
Bozzo, E., Bernardini, F., Ferrigno, C., et al. 2017, A&A, 608, A128
Bozzo, E., Ducci, L., & Falanga, M. 2021, MNRAS, 501, 2403
Burrows, D. N., Hill, J. E., Nousek, J. A., et al. 2005, Space Sci. Rev., 120, 165
Burrows, D. N., Kennea, J. A., Ghisellini, G., et al. 2011, Nature, 476, 421
Chernyakova, M., Lutovinov, A., Capitanio, F., Lund, N., & Gehrels, N. 2003, ATel, 157
Clark, D. J., Hill, A. B., Bird, A. J., et al. 2009, MNRAS, 399, L113
Clark, D. J., Sguera, V., Bird, A. J., et al. 2010, MNRAS, 406, L75
Coe, M. J., Fabregat, J., Negueruela, I., Roche, P., & Steele, I. A. 1996, MNRAS, 281, 333
Coleiro, A., & Chaty, S. 2013, ApJ, 764, 185
Coleiro, A., Chaty, S., Zurita Heras, J. A., Rahoui, F., & Tomsick, J. A. 2013, A&A, 560, A108
Corbet, R., & Krimm, H. 2013, ATel, 5126, 1
Corbet, R., Barbier, L., Barthelmy, S., et al. 2006, ATel, 779, 1
Corbet, R. H. D., Barthelmy, S. D., Baumgartner, W. H., et al. 2010, ATel, 2588
Cummings, J. R., Barthelmy, S. D., Beardmore, A. P., et al. 2011, GCN Circ., 11823, 1
Cummmings, J. R., Barthelmy, S. D., Chester, M. M., & Page, K. L. 2014, ATel, 6294, 1
D'Alessio, V., Piro, L., & Rossi, E. M. 2006, A&A, 460, 653
D'Elia, V., Krimm, H. A., Markwardt, C. B., et al. 2012, GCN Circ., 13964, 1

Darling, D. A. 1957, Ann. Math. Stat., 28, 823
de Pasquale, M., Barthelmy, S. D., Baumgartner, W. H., et al. 2010, ATel, 2661
Drave, S. P., Clark, D. J., Bird, A. J., et al. 2010, MNRAS, 409, 1220
Drave, S. P., Bird, A. J., Townsend, L. J., et al. 2012, A&A, 539, A21
Drave, S. P., Bird, A. J., Sidoli, L., et al. 2013, MNRAS, 433, 528
Ducci, L., Sidoli, L., Mereghetti, S., Paizis, A., & Romano, P. 2009, MNRAS, 398, 2152
Ducci, L., Sidoli, L., & Paizis, A. 2010, MNRAS, 408, 1540
Ducci, L., Doroshenko, V., Sasaki, M., et al. 2013, A&A, 559, A135
Ducci, L., Doroshenko, V., Romano, P., Santangelo, A., & Sasaki, M. 2014, A&A, 568, A76
Esposito, P., Rea, N., & Israel, G. L. 2021, Astrophys. Space Sci. Lib., 461, 97
Evans, P. A., Beardmore, A. P., Page, K. L., et al. 2007, A&A, 469, 379
Evans, P. A., Beardmore, A. P., Page, K. L., et al. 2009, MNRAS, 397, 1177
Evans, P. A., Willingale, R., Osborne, J. P., et al. 2010, A&A, 519, A102
Farinelli, R., Romano, P., Mangano, V., et al. 2012a, MNRAS, 424,2854
Farinelli, R., Ceccobello, C., Romano, P., & Titarchuk, L. 2012b, A&A, 538, A67
Farinelli, R., Ferrigno, C., Bozzo, E., & Becker, P. A. 2016, A&A, 591, A29
Fenimore, E. E., Palmer, D., Galassi, M., et al. 2003, AIP Conf. Ser., 662, 491
Ferrigno, C., Bozzo, E., Papitto, A., et al. 2014, A&A, 567, A77
Fiocchi, M., Sguera, V., Bazzano, A., et al. 2010, ApJ, 725, L68
Gamen, R., Barbà, R. H., Walborn, N. R., et al. 2015, A&A, 583, L4
Gehrels, N., Chincarini, G., Giommi, P., et al. 2004, ApJ, 611, 1005
Gimenez-Garcia, A., Shenar, T., Torrejon, J. M., et al. 2016, A&A, 591, A26
Goad, M. R., Tyler, L. G., Beardmore, A. P., et al. 2007, A&A, 476, 1401
González-Galán, A. 2015, arXiv e-prints [arXiv: 1503.01087]
Goossens, M. E., Bird, A. J., Drave, S. P., et al. 2013, MNRAS, 434, 2182
Götz, D., Schanne, S., Rodriguez, J., et al. 2006, ATel, 813, 1
Götz, D., Falanga, M., Senziani, F., et al. 2007, ApJ, 655, L101
Grebenev, S. A., & Sunyaev, R. A. 2007, Astron. Lett., 33, 149
Grupe, D., Kennea, J., Evans, P., et al. 2009, ATel, 2075, 1
Heise, J., Zand, J. I., Kippen, R. M., & Woods, P. M. 2001, in Gamma-ray Bursts in the Afterglow Era, eds. E. Costa, F. Frontera, & J. Hjorth (Berlin: Springer), 16,
Hubrig, S., Sidoli, L., Postnov, K., et al. 2018, MNRAS, 474, L27
in't Zand, J. J. M. 2005, A&A, 441, L1
in't Zand, J., Heise, J., Smith, M., et al. 1998, IAU Circ., 6840, 2
Kalberla, P. M. W., Burton, W. B., Hartmann D., et al. 2005, A&A, 440, 775
Kennea, J. A. 2006, AIP Conf. Ser., 840, 71
Kennea, J. A. 2015, J. High Energy Astrophys., 7, 105
Kennea, J. A., & Campana, S. 2006, ATel, 818, 1
Kennea, J. A., Pagani, C., Markwardt, C., et al. 2005, ATel, 599, 1
Kennea, J. A., Romano, P., Mangano, V., et al. 2011a, ApJ, 736, 22
Kennea, J. A., Romano, P., Mangano, V., et al. 2011b, ATel, 3242, 1
Kennea, J. A., Krimm, H. A., Romano, P., et al. 2014, ATel, 5980, 1
Kennea, J. A., Coe, M. J., Evans, P. A., et al. 2021, MNRAS, 508, 781
Kouveliotou, C., Meegan, C. A., Fishman, G. J., et al. 1993, ApJ, 413, L101
Kretschmar, P., Fürst, F., Sidoli, L., et al. 2019, New A Rev., 86, 101546
Krimm, H. A., & Romano, P. 2015, ATel, 7137, 1
Krimm, H. A., Barthelmy, S. D., Barbier, L., et al. 2007, ATel, 1265, 1
Krimm, H. A., Romano, P., & Sidoli L. 2009, ATel, 1971, 1
Krimm, H. A., Romano, P., Barthelmy, S. D., et al. 2011, ATel, 3780, 1
Krimm, H. A., Holland, S. T., Corbet, R. H. D., et al. 2013a, ApJS, 209, 14
Krimm, H. A., Mangano, V., Romano, P., et al. 2013b, ATel, 5398, 1
La Parola, V., Romano, P., Sidoli, L., et al. 2009, ATel, 1929, 1
La Parola, V., Cusumano, G., Romano, P., et al. 2010, MNRAS, 405, L66
Levan, A. J., Tanvir, N. R., Starling, R. L. C., et al. 2014, ApJ, 781, 13
Levine, A. M., & Corbet, R. 2006, ATel, 940, 1
Levine, A. M., Bradt, H. V., Chakrabarty, D., Corbet, R. H. D., & Harris, R. J. 2011, ApJS, 196, 6
Lin, D., Webb, N. A., & Barret, D. 2012, ApJ, 756, 27
Lorenzo, J., Negueruela, I., Castro, N., et al. 2014, A&A, 562, A18
Lubinski, P., Bel, M. G., von Kienlin, A., et al. 2005, ATel, 469, 1
Lutovinov, A., Rodrigues, J., Budtz-Jorgensen, C., Grebenev, S., & Winkler, C. 2004, ATel, 329, 1
Lutovinov, A., Revnivtsev, M., & Gilfanov, M. 2005, A&A, ATel, 444, 821
Lutovinov, A. A., Revnivtsev, M. G., Tsygankov, S. S., & Krivonos, R. A. 2013, MNRAS, 431, 327
Mangano, V., Romano, P., Sidoli, L., et al. 2008a, ATel, 1727, 1
Mangano, V., Baumgartner, W. H., Beardmore, A. P., et al. 2008b, GCN Circ., 8279, 1
Mangano, V., Barthelmy, S. D., Romano, P., et al. 2011a, ATel, 3453, 1
Mangano, V., Romano, P., Barthelmy, S. D., et al. 2011b, ATel, 3586, 1
Mangano, V., Romano, P., Ceccobello, C., & Farinelli, R. 2012, AIP Conf. Ser., 1505, 442
Margutti, R., Zaninoni, E., Bernardini, M. G., et al. 2013, MNRAS, 428, 729
Markwardt, C. B., & Krimm, H. A. 2006, ATel, 816, 1
Martínez-Núñez, S., Kretschmar, P., Bozzo, E., et al. 2017, Space Sci. Rev., 212, 59
Molkov, S., Mowlavi, N., & Goldwurm, A. 2003, ATel, 176, 1
Monet, D. G., Levine, S. E., Canzian, B., et al. 2003, AJ, 125, 984
Negueruela, I., & Schurch, M. P. E. 2007, AJ, 461, 631
Negueruela, I., Smith, D. M., Harrison, T. E., & Torrejón J. M. 2006, ApJ, 638, 982
Negueruela, I., Smith, D. M., Torrejón, J. M., & Reig, P. 2007, ESA SP, 622, 255
Negueruela, I., Torrejón, J. M., Reig, P., Ribó, M., & Smith, D. M. 2008, AIP Conf. Ser., 1010, 252
Nespoli, E., Fabregat, J., & Mennickent, R. E. 2008, A&A, 486, 911
Olausen, S. A., & Kaspi, V. M. 2014, ApJS, 212, 6
Paizis, A., & Sidoli, L. 2014, MNRAS, 439, 3439
Palmer, D., Barthelmy, S. D., Gehrels, N., et al. 2008, GCN Circ., 7946, 1
Papitto, A., Ferrigno, C., Bozzo, E., et al. 2013, Nature, 501, 517
Pellizza, L. J., Chaty, S., & Negueruela, I. 2006, A&A, 455, 653
Persi, P., Fiocchi, M., Tapia, M., et al. 2015, AJ, 150, 21
Press, W. H., Teukolsky, S. A., Vetterling, W. T., & Flannery, B. P. 1992, Numerical Recipes in C. The Art of Scientific Computing (Cambridge: Cambridge University Press)
Rahoui, F., Chaty, S., Lagage, P.-O., & Pantin, E. 2008, A&A, 484, 801
Reig, P. 2011, Ap&SS, 332, 1
Romano, P. 2014, GCN Circ., 16268, 1
Romano, P. 2015, J. High Energy Astrophys., 7, 126
Romano, P., Sidoli, L., Mangano, V., Mereghetti, S., & Cusumano, G. 2007, A&A, 469, L5
Romano, P., Sidoli, L., Mangano, V., et al. 2008a, ApJ, 680, L137
Romano, P., Sidoli, L., Mangano, V., et al. 2008b, ATel, 1435, 1
Romano, P., Sidoli, L., Mangano, V., et al. 2008c, ATel, 1466, 1
Romano, P., Guidorzi, C., Sidoli, L., et al. 2008d, ATel, 1659, 1
Romano, P., Cusumano, G., Sidoli, L., et al. 2008e, ATel, 1697, 1
Romano, P., Sidoli, L., Cusumano, G., et al. 2009a, MNRAS, 392, 45
Romano, P., Sidoli, L., Cusumano, G., et al. 2009b, MNRAS, 399, 2021
Romano, P., Sidoli, L., Cusumano, G., et al. 2009c, ApJ, 696, 2068
Romano, P., Sidoli, L., Mangano, V., et al. 2009d, ATel, 1920, 1
Romano, P., Sidoli, L., Krimm, H. A., et al. 2009e, ATel, 1961, 1
Romano, P., Sidoli, L., Krimm, H. A., et al. 2009f, ATel, 2044, 1
Romano, P., Sidoli, L., Vercellone, S., et al. 2009g, ATel, 2069, 1
Romano, P., Barthelmy, S., Margutti, R., et al. 2009h, ATel, 2102, 1
Romano, P., Barthelmy, S., Sidoli, L., et al. 2009i, ATel, 2191, 1
Romano, P., Barthelmy, S., Sidoli, L., et al. 2009j, ATel, 2279, 1
Romano, P., Sidoli, L., Ducci, L., et al. 2010a, MNRAS, 401, 1564
Romano, P., Krimm, H. A., Palmer, D. M., et al. 2010b, ATel, 2463, 1
Romano, P., Barthelmy, S. D., Baumgartner, W. H. et al. 2010c, ATel, 2520, 1
Romano, P., Cusumano, G., Baumgartner, W. H., et al. 2010d, ATel, 2662, 1
Romano, P., La Parola, V., Vercellone, S., et al. 2011a, MNRAS, 410, 1825
Romano, P., Mangano, V., Cusumano, G., et al. 2011b, MNRAS, 412, L30
Romano, P., Mangano, V., Cusumano, G., et al. 2011c, ATel, 3182, 1
Romano, P., Barthelmy, S. D., Esposito, P., et al. 2011d, ATel, 3235, 1
Romano, P., Mangano, V., Esposito, P., et al. 2012a, Mem. Soc. Astron. Italiana Suppl., 21, 210
Romano, P., Krimm, H. A., & Palmer, D. M. 2012b, ATel, 4040, 1
Romano, P., Barthelmy, S. D., Chester, M. M., et al. 2012c, ATel, 4095, 1
Romano, P., Barthelmy, S. D., Chester, M. M., et al. 2012d, ATel, 4148, 1
Romano, P., Barthelmy, S. D., Kennea, J. A., et al. 2012e, ATel, 4176, 1
Romano, P., Krimm, H., Sakamoto, T., et al. 2012f, ATel, 4275, 1
Romano, P., Krimm, H., Sbarufatti, B., et al. 2012g, ATel, 4276, 1
Romano, P., Barthelmy, S. D., Sakamoto, T., et al. 2012h, ATel, 4366, 1
Romano, P., Mangano, V., Ducci, L., et al. 2013a, Adv. Space Res., 52, 1593
Romano, P., Mangano, V., Ducci, L., et al. 2013b, Mem. Soc. Astron. Italiana, 84, 602
Romano, P., Barthelmy, S. D., Burrows, D. N., et al. 2013c, ATel, 4929, 1
Romano, P., Barthelmy, S. D., D'Elia, V., et al. 2013d, ATel, 4939, 1
Romano, P., Evans, P. A., Kennea, J. A., et al. 2013e, ATel, 5179, 1
Romano, P., Lien, A. Y., Evans, P. A., et al. 2013f, ATel, 5190, 1
Romano, P., Markwardt, C. B., Chester, M. M., et al. 2013g, ATel, 5388, 1
Romano, P., Krimm, H. A., Palmer, D. M., et al. 2014a, A&A, 562, A2
Romano, P., Ducci, L., Mangano, V., et al. 2014b, A&A, 568, A55
Romano, P., Barthelmy, S. D., Lien, A. Y., et al. 2014c, ATel, 6173, 1
Romano, P., Bozzo, E., Mangano, V., et al. 2014d, ATel, 6566, 1
Romano, P., Bozzo, E., Mangano, V., et al. 2015a, A&A, 576, L4
Romano, P., Barthelmy, S. D., Krimm, H. A., et al. 2015b, ATel, 7454
Romano, P., Bozzo, E., Esposito, P., et al. 2016, A&A, 593, A96
Sakamoto, T., Lamb, D. Q., Kawai, N., et al. 2005, ApJ, 629, 311
Sakamoto, T., Hullinger, D., Sato, G., et al. 2008, ApJ, 679, 570

Sakamoto, T., Barthelmy, S. D., Baumgartner, W. H., et al. 2011, GCN Circ., 11842, 1
Sbarufatti, B., Romano, P., Barthelmy, S. D., et al. 2021, ATel, 14924, 1
Sguera, V., Barlow, E. J., Bird, A. J., et al. 2005, A&A, 444, 221
Sguera, V., Hill, A. B., Bird, A. J., et al. 2007, A&A, 467, 249
Sguera, V., Bassani, L., Landi, R., et al. 2008, A&A, 487, 619
Sguera, V., Romero, G. E., Bazzano, A., et al. 2009, ApJ, 697, 1194
Sguera, V., Ducci, L., Sidoli, L., Bazzano, A., & Bassani, L. 2010, MNRAS, 402, L49
Shakura, N., Postnov, K., Kochetkova, A., & Hjalmarsdotter, L. 2012, MNRAS, 420, 216
Shakura, N., Postnov, K., Sidoli, L., & Paizis, A. 2014, MNRAS, 442, 2325
Sidoli, L., & Paizis, A. 2018, MNRAS, 481, 2779
Sidoli, L., Romano, P., Mereghetti, S., et al. 2007, A&A, 476, 1307
Sidoli, L., Romano, P., Mangano, V., et al. 2008a, ApJ, 687, 1230
Sidoli, L., Romano, P., Mangano, V., et al. 2008b, ATel, 1454, 1
Sidoli, L., Romano, P., Ducci, L., et al. 2009a, MNRAS, 397, 1528
Sidoli, L., Romano, P., Esposito, P., et al. 2009b, MNRAS, 400, 258
Sidoli, L., Romano, P., Mangano, V., et al. 2009c, ApJ, 690, 120
Sidoli, L., Tiengo, A., Paizis, A., et al. 2017, ApJ, 838, 133
Sidoli, L., Postnov, K. A., Belfiore, A., et al. 2019, MNRAS, 487, 420
Sidoli, L., Postnov, K., Tiengo, A., et al 2020, A&A, 638, A71
Smith, D. M., Main, D., Marshall, F., et al. 1997, IAU Circ., 6748, 2
Smith, D. M., Main, D., Marshall, F., et al. 1998, ApJ, 501, L181
Sota, A., Maíz Apellániz, J., Morrell, N. I., et al. 2014, ApJ, 211, 10
Sunyaev, R. A., Grebenev, S. A., Lutovinov, A. A., et al. 2003, ATel, 190, 1
Suzuki, D., Tristram, P. J., Kobara, S., et al. 2011, GCN Circ., 11824, 1
Swank, J. H., Smith, D. M., & Markwardt, C. B. 2007, ATel, 999, 1
Tomsick, J. A., Lingenfelter, R., Corbel, S., Goldwurm, A., & Kaaret, P. 2004, ATel, 224, 1
Torrejón, J. M., Negueruela, I., Smith, D. M., & Harrison, T. E. 2010, A&A, 510, A61
Vijapurkar, J., & Drilling, J. S. 1993, ApJS, 89, 293
Walter, R., & Zurita Heras, J. 2007, A&A, 476, 335
Walter, R., Lutovinov, A. A., Bozzo, E., & Tsygankov, S. S. 2015, A&ARv, 23, 2
Watson, M. G., Schröder, A. C., Fyfe, D., et al. 2009, A&A, 493, 339
Yamauchi, S., Aoki, T., Hayashida, K., et al. 1995, PASJ, 47, 189
Ziaeepour, H., Burrows, D. N., Campana, S., et al. 2006, GCN Circ., 5687, 1
Zurita Heras, J. A., & Chaty, S. 2009, A&A, 493, L1

Appendix A: Supplementary tables and figures

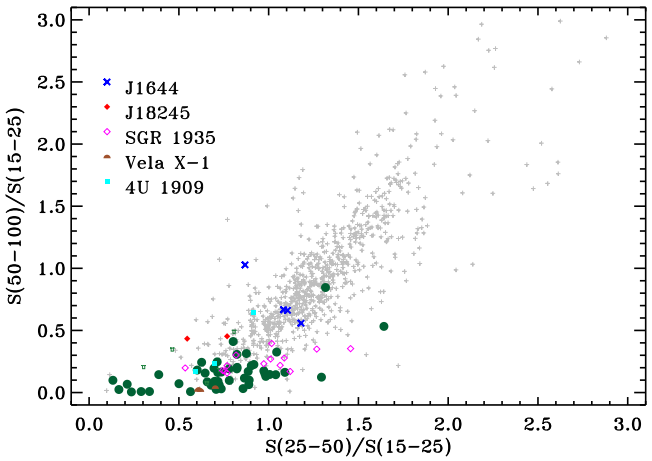

Fig. A.1. Energetics. Comparison of energetics of GRB (grey), SFXT (dark green filled circles, with green empty hats representing 3σ upper limits) and other prototypical transients: the TDE Swift J164449.3+573451 (J1644, blue X), the MSP IGRJ 18245−2452 (J18245, filled red diamonds), see Table A.1, the magnetar SGR 1935+2154 (SGR1935, empty magenta diamonds), and the two supergiant HMXBs Vela X-1 (filled upper half circles) and 4U 1909+07 (J1909, filled cyan squares), see Table A.2.

Table A.1. *Swift* data for Swift J164449.3+573451 and IGRJ 18245−2452.

Name	Trigger					References		Type of
	N[a]	#[b]	*S/N*[c]	UT Date	UT Time	Discovery	Refereed	Source
(1)	(2)	(3)	(4)	(5)	(6)	(7)	(8)	(9)
Swift J164449.3+573451	1	450158	7.60	2011-03-28	12:57:45	1,2	3	TDE
	2	450161	6.57	2011-03-28	13:40:41	4,2	3	
	3	450257	10.73	2011-03-29	18:26:25	5	3	
	4	450258	11.85	2011-03-29	19:57:45	5	3	
IGRJ 18245−2452	1	552336	5.86	2013-03-30	02:22:21	6,7	8	MSP
	2	552369	8.10	2013-03-30	15:10:37		8	

Notes. [(a)] Progressive number of BAT trigger. [(b)] BAT Trigger number. [(c)] On-board significance of detections of BAT trigger in units of σ.

References. (1) Cummings et al. (2011); (2) Kennea et al. (2011b); (3) Burrows et al. (2011); (4) Suzuki et al. (2011); (5) Sakamoto et al. (2011); (6) Barthelmy et al. (2013); (7) Romano et al. (2013c); (8) Papitto et al. (2013).

Table A.2. *Swift* data for other transients.

Name	Trigger					Trigger				
	N[a]	#[b]	*S/N*[c]	UT Date	UT Time	N[a]	#[b]	*S/N*[c]	UT Date	UT Time
SGR 1935+2154	1	603488	14.89	2014-07-05	09:32:49	9	701590	26.48	2016-06-26	13:54:31
(magnetar)	2	632159	16.47	2015-02-22	12:31:11	10	933083	11.11	2019-11-04	06:34:00
	3	686443	9.21	2016-05-16	20:49:47	11	933276	15.03	2019-11-05	00:08:58
	4	686761	24.16	2016-05-18	09:09:24	12	933285	23.89	2019-11-05	01:36:26
	5	686842	7.01	2016-05-19	05:41:26	13	968211	19.26	2020-04-27	18:26:20
	6	687123	6.93	2016-05-21	20:01:47	14	968212	19.17	2020-04-27	18:33:00
	7	687124	14.02	2016-05-21	20:23:42	15	1108538	22.93	2022-05-30	20:32:27
	8	701182	21.52	2016-06-23	19:24:40					
Vela X-1	1	500100	16.84	2011-08-12	06:38:04	3	618634	16.14	2014-11-14	21:11:12
(SgHMXB)	2	579975	12.64	2013-12-02	12:40:41	4	779762	25.6	2017-10-17	17:38:10
4U 1909+07	1	156561	5.57	2005-09-23	02:12:48	3	292965	8.26	2007-10-03	14:04:46
(SgHMXB)	2	157253	5.63	2005-09-27	07:02:56					

Notes. [(a)] Progressive number of BAT trigger. [(b)] BAT Trigger number. [(c)] On-board significance of detections of BAT trigger in units of σ.